



1 **Drivers of diffusive lake CH₄ emissions on daily to multi-year time scales**

2 Joachim Jansen^{1,2}, Brett F. Thornton^{1,2}, Alicia Cortes³, Jo Snöäl⁴, Martin Wik^{1,2}, Sally MacIntyre³
3 and Patrick M. Crill^{1,2}

4
5
6

7 ¹Department of Geological Sciences, Stockholm University, Stockholm, Sweden

8 ²Bolin Centre for Climate Research, Stockholm, Sweden

9 ³Marine Science Institute, University of California at Santa Barbara, Santa Barbara, USA

10 ⁴Department of Geography, University of Exeter, Exeter, UK

11

12 Corresponding author: Joachim Jansen (joachim.jansen@geo.su.se)



13 **Abstract**

14 Lakes and reservoirs are important emitters of climate forcing trace gases. Various environmental drivers
15 of the flux, such as temperature and wind speed, have been identified, but their relative importance
16 remains poorly understood. Here we use an extensive field dataset to disentangle physical and
17 biogeochemical controls on the turbulence-driven diffusive flux of methane (CH_4) on daily to multi-year
18 timescales. We compare 8 years of floating chamber fluxes from three small, shallow subarctic lakes
19 (2010–2017, $n = 1306$) with fluxes computed using 9 years of surface water concentration measurements
20 (2009–2017, $n = 606$) and a small-eddy surface renewal model informed by in situ meteorological
21 observations. Chamber fluxes averaged $6.9 \pm 0.3 \text{ mg m}^{-2} \text{ d}^{-1}$ and gas transfer velocities (k_{600}) from the
22 chamber-calibrated surface renewal model averaged $4.0 \pm 0.1 \text{ cm h}^{-1}$. We find robust ($R^2 \geq 0.93$, $p < 0.01$)
23 Arrhenius-type temperature functions of the CH_4 flux ($E_a' = 0.90 \pm 0.14 \text{ eV}$) and of the surface CH_4
24 concentration ($E_a' = 0.88 \pm 0.09 \text{ eV}$). Chamber derived gas transfer velocities tracked the power-law wind
25 speed relation of the model ($k \propto u^{3/4}$). While the flux increased with wind speed, during storm events
26 ($U_{10} \geq 6.5 \text{ m s}^{-1}$) emissions were reduced by rapid water column degassing. Spectral analysis revealed
27 that on timescales shorter than a month emissions were driven by wind shear, but on longer timescales
28 variations in water temperature governed the flux, suggesting emissions were strongly coupled to
29 production. Our findings suggest that accurate short- and long term projections of lake CH_4 emissions
30 can be based on distinct weather- and climate controlled drivers of the flux.



31 1. Introduction

32 Inland waters are an important source of the radiatively active trace gas methane (CH₄) to the
33 atmosphere (Bastviken et al., 2011; Cole et al., 2007). A significant portion of sediment-produced CH₄
34 reaches the atmosphere by turbulence-driven diffusion-limited gas exchange (Bastviken et al., 2004; Wik
35 et al., 2016b) (hereafter abbreviated to ‘diffusive fluxes’). Traditionally, diffusive fluxes are measured
36 with floating chambers (Bastviken et al., 2004) but gas exchange models are increasingly used, for
37 example to estimate annual emissions on regional scales (Holgerson and Raymond, 2016; Weyhenmeyer
38 et al., 2015). Fluxes computed with modelled gas transfer velocities agree to a certain extent with
39 floating chambers and the eddy covariance technique in short-term intercomparison campaigns
40 (Bartosiewicz et al., 2015; Crill et al., 1988; Erkkilä et al., 2018). However, long-term comparisons are
41 needed to test the validity of flux-driver relations on which models are based across a wider range of
42 meteorological conditions, and to identify weather- and climate related controls on the flux that are
43 appropriate for seasonal assessments. Considering the increased use of process-based approaches in
44 regional emission estimates (DelSontro et al., 2018; Tan and Zhuang, 2015), understanding the
45 mechanisms that drive the components of the diffusive flux is imperative to improving emission budgets.

47 1.1 Drivers of diffusive CH₄ emissions

48 Diffusive fluxes at the air-water interface can be modelled as:

$$F = k(C_{aq} - C_{air,eq}) \quad [1]$$

49 The flux F [mg m⁻² d⁻¹] depends on the concentration difference across a thin layer immediately below
50 the air-water interface ($\Delta[\text{CH}_4]$ in mg m⁻³), which upper boundary is in equilibrium with the atmosphere
51 ($C_{air,eq}$) and base represents the bulk liquid (C_{aq}), and is limited by the gas transfer velocity k [m d⁻¹]
52 (Wanninkhof, 1992). k has been conceptualized as characterizing transfer across the diffusive boundary
53 layer, although other models envision a surface renewal approach in which parcels of water
54 intermittently are in contact with the atmosphere and k depends on the frequency of these renewal
55 events (Csanady, 2001; Lamont and Scott, 1970).

57 The gas transfer coefficient depends on turbulence caused by wind shear and convection and on the
58 molecular diffusivity of the dissolved gas (see MacIntyre et al., 1995 for an overview of the
59 thermodynamic and kinetic drivers of k). In a stratified water column the force of buoyancy counteracts
60 that of wind shear, and gases may accumulate below a shallow upper mixing layer (MacIntyre et al.,
61 2010). Conversely, thermal convection as a result of surface cooling can deepen the mixed layer and
62 transfer stored gas to the surface (Crill et al., 1988; Eugster et al., 2003), and enhance emissions at night
63 when the surface cools despite low wind speeds (Heiskanen et al., 2014; Podgrajsek et al., 2014b;
64 Poindexter et al., 2016). While progress has been made in understanding how the components of k vary
65 as a function of turbulence (Tedford et al., 2014) and other factors, such as lake morphology and
66 distance to the shoreline (Read et al., 2012; Schilder et al., 2013; Vachon and Prairie, 2013), the temporal
67 variability and drivers of $\Delta[\text{CH}_4]$ remain poorly resolved (Loken et al., 2019; Natchimuthu et al., 2016).

69 CH₄ emissions to the atmosphere also depend on the rates of methane metabolism regulated by
70 substrate availability and temperature-dependent shifts in enzyme activity and microbial community



71 structure (Borrel et al., 2011; McCalley et al., 2014; Tveit et al., 2015). Arrhenius-type relationships of
72 CH₄ fluxes have emerged from field studies (DelSontro et al., 2018; Natchimuthu et al., 2016; Wik et al.,
73 2014) and across latitudes and aquatic ecosystem types in synthesis reports (Rasilo et al., 2015; Yvon-
74 Durocher et al., 2014). However, the temperature sensitivity is modulated by biogeochemical factors
75 that differ between lake ecosystems, such as nutrient content (Davidson et al., 2018; Sepulveda-Jauregui
76 et al., 2015), methanotrophic activity (Duc et al., 2010; Lofton et al., 2014), predominant emission
77 pathway (DelSontro et al., 2016; Jansen et al., 2019) and warming history (Yvon-Durocher et al., 2017). In
78 lakes, the air-water concentration difference driving the flux (Eq. 1) is further impacted by abiotic factors
79 that dissociate production from emission rates, such as hydrologic inputs of terrestrially produced CH₄
80 (Miettinen et al., 2015; Murase et al., 2003; Paytan et al., 2015), redistribution of dissolved gas in the
81 water column (DelSontro et al., 2017; Hofmann, 2013) and storage-and-release cycles associated with
82 transient stratification (Czikowsky et al., 2018; Jammet et al., 2017; Vachon et al., 2019). From these
83 interacting functional dependencies emerge complex responses of the flux to biotic and abiotic factors.

84
85 Disentangling the physical and biogeochemical drivers of the diffusive CH₄ flux remains a challenge. They
86 respond differently to slow and fast changes in meteorological covariates (Baldocchi et al., 2001;
87 Koebisch et al., 2015) such that different mechanisms may explain the diel and seasonal variability of the
88 flux. For example, temperature affects emissions through convective mixing on short timescales and
89 through the rate of sediment methanogenesis on longer timescales; the diurnal cycle of insolation may
90 have a limited effect on production because the heat capacity of the water buffers the temperature
91 signal (Fang and Stefan, 1996). Similar phase lags and amplifications may lead to hysteretic flux patterns,
92 such as cold season emission peaks due to hypolimnetic storage in dimictic lakes (Encinas Fernández et
93 al., 2014; López Bellido et al., 2009) or thermal inertia of lake sediments (Zimov et al., 1997). Spectral
94 analysis of the flux and its components can improve our understanding of the flux variability by
95 quantifying how much power is associated with key periodicities (Baldocchi et al., 2001).

96
97 Here we present a high-resolution, long-term dataset (2010–2017) of turbulence-driven diffusion-limited
98 CH₄ fluxes from three subarctic lakes estimated with floating chambers ($n = 1306$) and a gas exchange
99 model informed by in situ meteorological observations and surface water concentrations ($n = 535$). We
100 use a surface renewal model and Arrhenius relationships of $\Delta[\text{CH}_4]$ to disentangle the abiotic and biotic
101 effects of temperature on the flux. We then use stochastic tools to estimate the importance of these and
102 other flux controls on different timescales.



103 **2. Materials and Methods**

104 **2.1 Field site**

105 We monitored CH₄ emissions from three subarctic lakes of post-glacial origin (Kokfelt et al., 2010),
106 located on the Stordalen Mire in northern Sweden (68°21' N, 19°02' E, Fig. 1), a peatland underlain by
107 discontinuous permafrost (Malmer et al., 2005). The mire (350 m a.s.l.) is part of a catchment that
108 connects Mt. Vuoskoåiveh (920 m a.s.l.) in the south to Lake Torneträsk (341 m a.s.l.) in the north
109 (Lundin et al., 2016; Olefeldt and Roulet, 2012). Villasjön is the largest and shallowest of the lakes (0.17
110 km², 1.3 m max. depth) and drains through water-logged fens into a stream feeding Mellersta Harrsjön
111 and Inre Harrsjön, which are 0.011 and 0.022 km² in size and have maximum depths of 6.7 m and 5.2 m,
112 respectively (Wik et al., 2011). The lakes are normally ice-free from the beginning of May through the
113 end of October. Manual observations were generally conducted between mid-June and the end of
114 September. Diffusion accounts for 17%, 52% and 34% of the ice-free CH₄ flux in Villasjön, Inre and
115 Mellersta Harrsjön, respectively, with the remainder being emitted via ebullition (2010–2017; Jansen et
116 al., 2019).

117

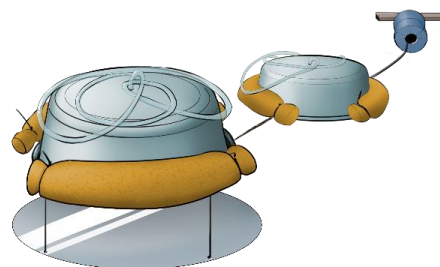
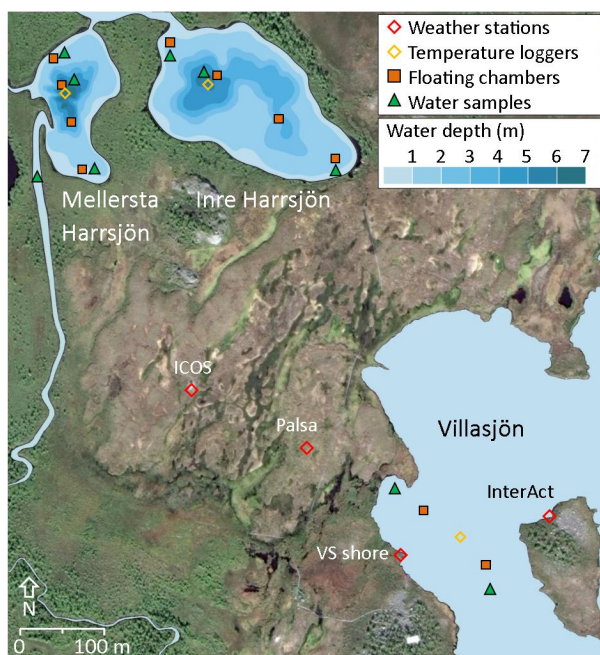


Figure 1 – Map of the Stordalen Mire field site (left). Chamber and sampling locations are shown as they were in 2015–2017. A schematic of the floating chamber pairs is shown to the right. Lake bathymetry from Wik et al. (2011). Satellite imagery: ©Google, DigitalGlobe, 2017.

118



119 2.2 Floating chambers

120 We used floating chambers to directly measure the turbulence-driven diffusive CH₄ flux across the air-
121 water interface (Fig. 1). They consisted of plastic tubs covered with aluminium tape to reflect incoming
122 radiation and were equipped with polyurethane floaters and flexible sampling tubes capped at one end
123 with 3-way stopcocks (Bastviken et al., 2004). Depending on flotation depth each chamber covered an
124 area between 610 and 660 cm² and contained a headspace of 4 to 5 litres. A plastic shield was mounted
125 underneath one chamber of each pair to deflect methane bubbles rising from the sediment. Every 1–2
126 weeks during the ice-free seasons of 2010 to 2017 2–4 chamber pairs were deployed in Villasjön and 4–7
127 chamber pairs in Inre and Mellersta Harrsjön in different depth zones (Fig. 1). The number of chambers
128 and deployment intervals exceeded the minimum needed to resolve the spatiotemporal variability of the
129 flux (Wik et al., 2016a). Over a 24 hour period 2–4 60 mL headspace samples were collected from each
130 chamber using polypropylene syringes and the flotation depth and air temperature were noted in order
131 to calculate the headspace volume. The 24-hour deployment period was chosen to compute fluxes over
132 timescales which integrate diel variations in the gas transfer velocity (Bastviken et al., 2004).

133
134 The fluxes reported here are from the shielded chambers only. To check that the shields were not
135 reducing fluxes from turbulent processes such as convection, we compared fluxes from shielded and
136 unshielded chambers on days when the lake mean bubble flux was <1% of the lake mean diffusive flux
137 (bubble traps, 2009–2017; Jansen et al., 2019; Wik et al., 2013). Averaged over the three lakes, the
138 difference was statistically significant ($F_{ch,unsh} - F_{ch,sh} = 0.20 \pm 0.16 \text{ mg m}^{-2} \text{ d}^{-1}$ ($n = 58$) (mean \pm 95% CI)) but
139 only a 6% difference from mean fluxes. Conversely, some types of floating chambers can enhance gas
140 transfer by creating artificial turbulence when dragging through the water (Matthews et al., 2003;
141 Vachon et al., 2010; Wang et al., 2015). The effect appears to be negligible for chambers of the design,
142 size and flotation depth used in this study (acoustic Doppler velocimeter measurements, Ribas-Ribas et
143 al., 2018).

144 145 2.3 Water samples

146 Surface water samples were collected at a depth of 0.2–0.4 m at 2–3 different locations in each lake (Fig.
147 1), at one to two-week intervals from June to October. Samples were collected from shore with a 4 m
148 Tygon tube attached to a floater to avoid disturbing the sediments (2009–2014) and from a rowing boat
149 over the deepest points of Inre and Mellersta Harrsjön (2010–2017) and at shallows (<1 m water depth)
150 on either end of the lakes (2015–2017) using a 1.2 m Tygon tube. In addition, water samples were
151 collected at the deepest point of Inre and Mellersta Harrsjön at 1 m intervals down to 0.1 m from the
152 sediment surface with a 7.5 m fluorinated ethylene propylene (FEP) tube. 60 mL polypropylene syringes
153 were rinsed thrice with sample water before duplicate bubble-free samples were collected, and were
154 capped with airtight 3-way stopcocks. 30 mL samples were equilibrated with 30 mL headspace and
155 shaken vigorously by hand for 2 minutes (2009–2014) or on a mechanical shaker at 300 rpm for 10
156 minutes (2015–2017). Prior to 2015, lab air – with a predetermined CH₄ content – was used as
157 headspace. From 2015 on we used an N₂ 5.0 headspace (Air Liquide). Water sample conductivity was
158 measured over the ice-free season of 2017 ($n = 323$) (S230, Mettler-Toledo).



159 **2.4 Concentration measurements**

160 Gas samples were analysed within 24 hours after collection at the Abisko Scientific Research Station, 10
 161 km from the Stordalen Mire. Sample CH₄ contents were measured on a Shimadzu GC-2014 gas
 162 chromatograph which was equipped with a flame ionization detector (GC-FID) and a 2.0 m long, 3 mm ID
 163 stainless steel column packed with 80/100 mesh HayeSep Q and used N₂ >5.0 as a carrier gas (Air
 164 Liquide). For calibration we used standards of 2.059 ppm CH₄ in N₂ (Air Liquide). 10 standard
 165 measurements were made before and after each run. After removing the highest and lowest values,
 166 standard deviations of the standard runs were generally less than 0.25%.

167
 168 **2.5 Water temperature and pressure loggers**

169 Water temperature was measured every 15 minutes from 2009 to 2018 with temperature loggers (HOBO
 170 Water Temp Pro v2, Onset Computer) in Villasjön and at the deepest locations within Inre and Mellersta
 171 Harrsjön. Sensors monitored the surface water in all lakes at 0.1, 0.3, 0.5, 1.0 m depth, and further at
 172 3.0, 5.0 m (IH and MH) and at 6.7 m (MH) at the deep points. Sensors were intercalibrated prior to
 173 deployment in a well-mixed water tank, and by comparing readouts just before ice-on when the water
 174 column was isothermal. In this way a precision of <0.05 °C was achieved. The bottom sensors were
 175 buried in the surface sediment and were excluded from in situ intercalibration. Water pressure was
 176 measured in Mellersta Harrsjön (5.5 m) with a HOBO U20 Water Level logger (Onset Computer).

177
 178 **2.6 Meteorology**

179 Meteorological data was collected from four different masts on the Mire (Fig. 1), and collectively covered
 180 a period from June 2009 to October 2017 with half-hourly measurements of wind speed, air
 181 temperature, relative humidity, air pressure and irradiance (Table 1). Wind speed was measured with 3D
 182 sonic anemometers at the Palsa tower (z = 2.0 m), the Villasjön shore tower (z = 2.9 m), at the InterAct
 183 Lake tower (z = 2.0 m) and at the Integrated Carbon Observation System (ICOS) site (z = 4.0 m). Air
 184 temperature and relative humidity were measured at the Palsa tower, at the Villasjön shore tower
 185 (Rotronic MP100a (2012–2015) / Vaisala HMP155 (2015–2017)) and at the InterAct lake tower. Incoming
 186 and outgoing shortwave and long wave radiation were monitored with net radiometers at the Palsa
 187 tower (Kipp & Zonen CNR1) and at the InterAct lake tower (Kipp & Zonen CNR4). Precipitation data was
 188 collected with a WeatherHawk 500 at the ICOS site. Overlapping measurements were cross-validated
 189 and averaged to form a single timeseries.

190
 191 **Table 1** – Location and instrumentation of meteorological observations on the Stordalen mire, 2009–2018.

| Identifier | Period | Location | Wind | Air temp. and humidity | Radiation | Ref. |
|-----------------------|---------|--------------------------------|---------------------------------------|---|-----------------------------------|-----------------------|
| Palsa tower | 2009-11 | 68°21'19.68"N 19° 2'52.44"E | C-SAT 3 <i>Campbell Scientific</i> | HMP-45C <i>Campbell Scientific</i> | CNR-1 <i>Kipp & Zonen</i> | Olefeldt et al., 2012 |
| Villasjön shore tower | 2012-18 | 68°21'14.58"N 19° 3'1.07"E | R3-50 <i>Gill</i> | MP100a, <i>Rotronic</i> HMP155, <i>Vaisala</i> | REBS Q7.1 <i>Campbell Sci.</i> | Jammet et al., 2015 |
| InterAct Lake tower | 2012-18 | 68°21'16.22"N 19° 3'14.98"E | uSonic 3 Scientific <i>Metek</i> | CS215 <i>Campbell Scientific</i> | CNR-4 <i>Kipp & Zonen</i> | x |
| ICOS site | 2013-18 | 68°21'20.59"N 19° 2'42.08"E | | Weatherhawk 500 <i>Campbell Scientific</i> | | x |



193 2.7 Computation of CH₄ storage and residence time

194 The amount of stored CH₄ (g CH₄ m⁻²) was computed by weighting and then adding each concentration
195 measurement by the volume of the 1 m depth interval within which it was collected. For the upper 2 m
196 of the two deeper lakes we separately computed storage in the vegetated littoral zone from near-shore
197 concentration measurements, as these values could be different from those further from shore due to
198 outgassing and oxidation during transport (DelSontro et al., 2017). We computed the average residence
199 time of a CH₄ molecule by dividing the amount stored by the lake mean surface flux. Residence times
200 computed with this approach should be considered upper limits, because we implicitly assumed that
201 removal processes other than surface emissions, such as microbial oxidation, were negligible or took
202 place at the sediment-water interface with minimal impact on water column CH₄.

204 2.8 Flux calculations

205 In order to calculate the chamber flux with Eq. 1 we estimated k_{ch} from the time-dependent equilibrium
206 chamber headspace concentration $C_{h,eq}(t)$ [mg m⁻³] (Bastviken et al., 2004):

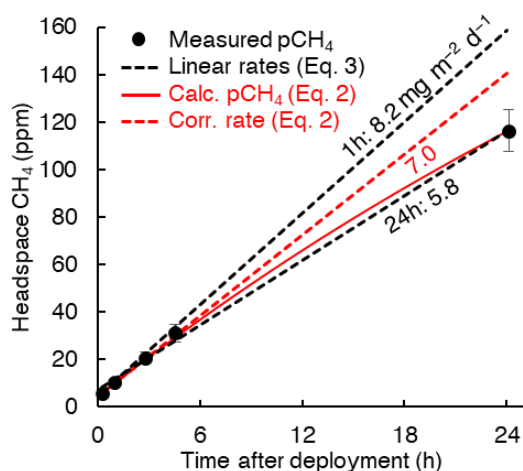
$$[C_{aq} - C_{h,eq}(t)] = [C_{aq} - C_{h,eq}(t_0)] e^{-\frac{K_H R T A}{V} k_{ch} t} \quad [2]$$

207 where K_H is Henry's law constant for CH₄ [mg m⁻³ Pa⁻¹] (Wiesenburg and Guinasso, 1979), R is the
208 universal gas constant [m³ Pa mg⁻¹ K⁻¹], T is the surface water temperature [K] and V and A are the
209 chamber volume [m³] and area [m²], respectively. This method accounts for gas accumulation in the
210 chamber headspace, which reduces the concentration gradient and limits the flux (Eq. 1) (Fig. 2). For a
211 subset of chamber measurements where simultaneous water concentration measurements were
212 unavailable we computed the flux from the headspace concentrations alone:

$$F = c_1 M \frac{\partial x_h}{\partial t} \frac{PV}{RTA} \quad [3]$$

213 where $\partial x_h / \partial t$ is the headspace mole fraction change [10⁻⁶ ppm d⁻¹], M is the molar mass of CH₄ (0.016
214 mg mol⁻¹), P is the air pressure [Pa], T is the air temperature [K]. Scalar c_1 corrects for accumulation of
215 CH₄ gas in the chamber headspace and increases over the deployment time. Comparing both chamber
216 flux calculation methods we find $c_1 = 1.21$ for 24 hour deployments (OLS, $R^2 = 0.85$, $n = 357$). Chambers
217 were sampled up to 4 times during deployment (at 10 minutes, 1–5 hours and 24 hours) which allowed
218 us to compute fluxes at different time intervals.

219
220 Figure 2 illustrates the importance of the headspace correction. The headspace-corrected flux (dashed
221 red line) equals the initial slope of Eq. 2 (solid red line) and is about 21% higher than the non-corrected
222 flux (lower dashed black line). However, both Eq. 2 (solid red line) and Eq. 3 with $c_1 = 1$ (dashed black
223 lines) fit the concentration data ($R^2 \geq 0.98$ for 94% of 24-hour flux measurements). This is partly because
224 the fluxes were low enough to keep headspace concentrations well below equilibrium with the water
225 column, and because on average, the gas transfer velocity deviated $\leq 10\%$ from its mean value over its
226 diel cycle (Fig. 7d). Short-term measurements (upper dashed black line) may omit the need for
227 headspace correction but can significantly overestimate the flux if – as in our study – initial chamber
228 deployment takes place during daytime and k or $\Delta[\text{CH}_4]$ follow a diurnal pattern (Bastviken et al., 2004).



229 **Figure 2** – Example of chamber headspace CH_4 concentrations versus deployment time. Measured
230 concentrations (dots) are averages from 2015–2017 (0.1h) and 2011 (1h–24h); error bars represent the
231 95% confidence intervals. Linear regressions (dashed black lines) show the rate increase over 1 hour (two
232 measurements) and over 24 hours (five measurements). The solid red line represents chamber
233 concentrations computed with Eq. 2 using multi-year mean values of $\Delta[\text{CH}_4]$ and k_{ch} (uncorrected for
234 headspace accumulation). The rate increase associated with the mean 24h flux corrected for headspace
235 accumulation is shown as a dashed red line (Eq. 1 with k_{ch} from Eq. 2, or Eq. 3 with $c_1 = 1.21$). Labels
236 denote fluxes calculated from the linear regression slopes (Eq. 3, black) and from Eq. 2 (red).

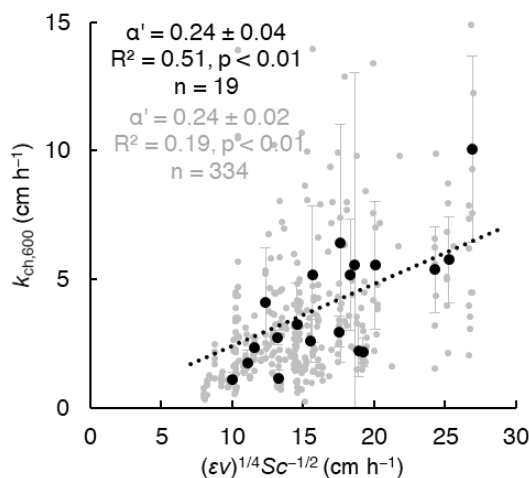


237 **2.9 Computing gas transfer velocities with the surface renewal model**

238 We used the surface renewal model (Lamont and Scott, 1970) formulated for small eddies at Reynolds
 239 numbers >500 (MacIntyre et al., 1995; Theofanous et al., 1976) to estimate k :

$$k_{mod} = \alpha(\epsilon\nu)^{\frac{1}{4}} Sc^{-\frac{1}{2}} \quad [4]$$

240 where the hydrodynamic and thermodynamic forces driving gas transfer are expressed, respectively, as
 241 the dissipation of turbulent kinetic energy (TKE), ϵ [m^2s^{-3}], and the dimensionless Schmidt number Sc ,
 242 defined as the ratio of the kinematic viscosity ν [m^2s^{-1}] to the free solution diffusion coefficient D_0 [m^2s^{-1}]
 243 (Jähne et al., 1987; Wanninkhof, 2014). The scaling parameter α has a theoretical value of 0.37 (Katul et
 244 al., 2018), but is often estimated empirically (α') to calibrate the model (e.g. Wang et al., 2015). To allow
 245 for a qualitative comparison between model and chamber fluxes we regressed k_{ch} (floating chambers)
 246 onto $(\epsilon\nu)^{\frac{1}{4}} Sc^{-\frac{1}{2}}$ (surface renewal model, half-hourly values of k_{mod} averaged over each chamber
 247 deployment period), and determined $\alpha' = 0.24 \pm 0.04$ (mean \pm 95% CI, $n = 334$) (Fig. 3). When comparing
 248 k -values we normalized to a Schmidt number of 600 (CO_2 at 20 °C) (Wanninkhof, 1992): $k_{600} =$
 249 $(600/Sc)^{-0.5}k$. To enable comparison with published wind- k relations we calculated the wind speed at
 250 10 m (U_{10}) from the anemometer datasets following Smith (1988), assuming a neutral atmosphere.



251
 252
 253
 254
 255
 256
 257
 258
 259
 260
 261
 262
 263
 264
 265
 266 **Figure 3** – Comparison between gas transfer velocities from floating chambers (Eq. 2) and the surface
 267 renewal model (Eq. 4 with $\alpha' = 1$ and $Sc = 600$, half-hourly values averaged over each chamber
 268 deployment period). Grey dots are individual chamber deployments and black dots represent multi-
 269 chamber means for each weekly deployment in 2016 and 2017, when concentration measurements
 270 were taken simultaneously with, and in close proximity to the chamber measurements. Intercepts of the
 271 linear regressions (lines) were fixed at 0. Error bars represent 95% confidence intervals of the means.

272
 273 We used a parametrization by Tedford et al. (2014) based on Monin-Obukhov similarity theory to
 274 estimate the TKE dissipation rate at half-hourly time intervals:

$$\epsilon = \begin{cases} 0.56 u_{*w}^3 / \kappa z + 0.77\beta & \text{if } \beta > 0 \\ 0.6 u_{*w}^3 / \kappa z & \text{if } \beta \leq 0 \end{cases} \quad [5]$$



275 where u_{*w} is the water friction velocity [m s^{-1}], κ is the von Kármán constant, z is the depth below the
276 water surface (here set to 0.15 m, the depth for which Eq. 5 was calibrated). We determined u_{*w} from
277 the air friction velocity u_{*a} assuming equal shear stresses (τ) on either side of the air-water interface;
278 $\tau = \rho_a u_{*a}^2 = \rho_w u_{*w}^2$ (MacIntyre and Melack, 1995), and taking into account atmospheric stability
279 (Imberger, 1985; MacIntyre et al., 2014; Tedford et al., 2014). β is the buoyancy flux [$\text{m}^2 \text{s}^{-3}$], which
280 accounts for turbulence generated by convective mixing (Imberger, 1985):

$$\beta = \frac{\alpha_T g Q_{eff}}{c_{pw} \rho_w} \quad [6]$$

281 where α_T is the thermal expansion coefficient [$\text{m}^3 \text{K}^{-1}$] (Kell, 1975), g is the standard gravity [m s^{-2}], c_{pw}
282 [$\text{J kg}^{-1} \text{K}^{-1}$] is the water specific heat and ρ_w [kg m^{-3}] is the water density, calculated from the water
283 temperature and corrected for dissolved solids using conductivity measurements and a conversion factor
284 of $0.57 \text{ g kg}^{-1} / \text{mS cm}^{-1}$. Q_{eff} [W m^{-2}] represents the net heat flux into the surface mixed layer and is the
285 sum of net shortwave and long-wave radiation and sensible and latent heat fluxes. We used Beer's Law
286 to compute penetration of radiation into the water column across seven wavelength bands (Jellison and
287 Melack, 1993). Attenuation of the visible portion of the spectrum was computed from the Secchi depth
288 (Karlsson et al., 2010; Wik et al., 2018) with the inverse relationship from Idso and Gilbert (1974). We
289 further computed outgoing component of the net longwave radiation (LW_{net}) using the Stefan-Boltzmann
290 law: $LW_{out} = \sigma T^4$, where σ is the Stefan-Boltzmann constant ($5.67 \times 10^{-8} \text{ W m}^{-2} \text{K}^{-4}$) and T is the surface
291 water temperature in K. For periods where we did not have longwave radiation data we assumed $LW_{net} =$
292 -50 W m^{-2} . Sensible and latent heat fluxes were computed with bulk aerodynamic formula described in
293 MacIntyre et al. (2002). Both Q_{eff} and β are here defined as positive when the heat flux is directed out
294 of the water, for example when the surface water cools.

295
296 Direct measurements of turbulent dissipation rates in a small Arctic lake (1 m depth, 0.005 km^2) show
297 that Equation 5 well characterizes near-surface turbulence in small, sheltered water bodies similar to the
298 lakes studied here (MacIntyre et al., 2018). Eq. 5 underestimates the dissipation-suppressing effects of
299 stratification of the upper water column at buoyancy frequencies ($N = \sqrt{g/\rho_w \times d\rho_w/dz}$) exceeding 25
300 cycles per hour (MacIntyre et al., 2018). However, in the current dataset such periods of strong
301 stratification ($N > 25$ cph) were observed $< 3\%$ of the time.

302

303 **2.10 Calculation of binned means**

304 We binned data to assess correlations between the flux and environmental covariates. Half-hourly values
305 of water temperature and wind speed were averaged over the deployment period of each chamber
306 (fluxes) and over 24 hours prior to the collection of each water sample (concentrations). The 24 hour
307 averaging period was chosen based on the mean residence time of a CH_4 molecule in the lake water
308 column. Parameters of interest (fluxes, concentrations and k) were then binned in 10 day, 1°C and 0.5 m
309 s^{-1} bins to obtain relationships with time, water temperature and wind speed, respectively. For this
310 calculation, lake-specific variables such as water temperature were normalized by lake to obtain a single
311 timeseries (divided by the lake mean, multiplied by the overall mean).



312 **2.11 Calculation of the empirical activation energy**

313 Chamber and modelled fluxes as well as surface concentrations were fitted to an Arrhenius-type
314 temperature function (e.g. Wik et al., 2014; Yvon-Durocher et al., 2014):

$$F = e^{-E_a'/k_B T + b} \quad [7]$$

315 where k_B is the Boltzmann constant (8.62×10^{-5} eV K⁻¹) and T is the water temperature in K. The
316 empirical activation energy (E_a' , in electron volts (eV), 1 eV = 96 kJ mol⁻¹) was computed with a linear
317 regression of natural logarithm of the fluxes and concentrations onto the inverse temperature (1/K), of
318 which b is the intercept.

319

320 **2.12 Timescale analysis: power spectra and climacogram**

321 We computed power spectra for near-continuous timeseries of the water- and air temperature and the
322 wind speed according to Welch's method (pwelch in MATLAB 2018a), which splits the signal into
323 overlapping sections and applies a cosine tapering window to each section (Hamming, 1989). Data gaps
324 were filled by linear interpolation. We removed the linear trend from original timeseries to reduce red
325 noise, and block-averaged spectra (8 segments with 50% overlap) to suppress aliasing at higher
326 frequencies. We normalized the spectra by multiplying by the natural frequency and dividing by the
327 variance of the original timeseries (Baldochi et al., 2001).

328

329 We evaluated discontinuous timeseries with a climacogram, an intuitive way to visualize a continuum of
330 variability (Dimitriadis and Koutsoyiannis, 2015). It displays the change of the standard deviation (σ) with
331 averaging timescale (t_{avg}) in double-logarithmic space. Variables of interest were normalized by lake to
332 create a single time-series at half-hourly resolution (i.e. 48 entries for each 24-hour chamber flux). To
333 compute each standard deviation ($\sigma(t_{avg})$) data was binned according to averaging timescale, which
334 ranged from 30 minutes to 1 year. Because of the discontinuous nature of the datasets, n bins were
335 distributed randomly across the time series. We chose $n = 100000$ to ensure that the 95% confidence
336 interval of the standard deviation at the smallest bin size was less than 1% of the value of σ (Sheskin,
337 2007). To allow for comparison between variables we normalized each σ -series by its smallest-bin value:
338 $\sigma_{norm} = \sigma/\sigma_{init}$. For timescales < 1 week we used 1-hour chamber observations. We use the climacogram
339 specifically to test whether the variability of the diffusive CH₄ flux is enveloped by hydrometeorological
340 variability, as for terrestrial ecosystem processes (Pappas et al., 2017).

341

342 **2.13 Statistics**

343 We used Analysis of Variance (ANOVA) and the t-test to compare means of different groups. The use of
344 means, rather than medians was necessary because annual emissions can be determined by rare, high-
345 magnitude emission events. Parametric tests were justified because of the large number of samples in
346 each analysis, in accordance with the central limit theorem. Linear regressions were performed with the
347 ordinary least squares method (OLS): reported p -values refer to the significance of the regression slope.
348 Non-linear regressions were optimized with the Levenberg-Marquardt algorithm for non-linear least
349 squares with confidence intervals based on bootstrap replicates ($n = 1999$). Computations were done in
350 MATLAB 2018a and in PAST v3.25 (Paleontological Statistics software package) (Hammer et al., 2001).



351 **3. Results**

352 **3.1 Measurements and models**

353 Chamber fluxes averaged $6.9 \text{ mg m}^{-2} \text{ d}^{-1}$ (range 0.2–32.2, $n = 1306$) and closely tracked the temporal
 354 evolution of the surface water concentrations (mean 11.9 mg m^{-3} , range 0.3–120.8, $n = 606$), with the
 355 higher values in each lake measured in the warmest months (July and August, Fig 4a,e). As expected,
 356 diffusive fluxes increased with wind speed and water temperature (Fig 4b,c). Reduced emissions were
 357 measured in the shoulder months (June and September) and were associated with lower water
 358 temperatures. We also observed abrupt reductions of the flux at wind speeds lower than 2 m s^{-1} and
 359 higher than 6.5 m s^{-1} . Surface water concentrations generally increased with temperature and peaked in
 360 the summer months, but unlike the chamber fluxes they decreased with increasing wind speed (Fig.
 361 4f,g). Relationships with wind speed were approximately linear, while relationships with temperature
 362 fitted an Arrhenius-type exponential function (Eq. 7). Activation energies were not significantly different
 363 between the surface water and sediment temperature ($E_a' = 0.90 \pm 0.14 \text{ eV}$, $R^2 = 0.93$, $E_a' = 1.00 \pm 0.17$,
 364 $R^2 = 0.93$, respectively, mean \pm 95% CI). The fluxes, concentrations, and the wind speed were non-
 365 normally distributed (Fig. 4d,h,o). Surface water temperatures (0.1–0.5 m) were normally distributed for
 366 each individual month of the ice-free season (Fig. 4n), but the composite distribution was bimodal.

367
 368 Fluxes computed with the surface renewal model (Eq. 1 using k_{mod}) closely resembled the chamber fluxes
 369 (Eq. 3) in terms of temporal evolution (Fig. 4a) and correlation with environmental drivers (Fig. 4b,c).
 370 Despite the model's calibration with a subset of the chamber data, model fluxes were higher than the
 371 chamber fluxes in all lakes (Table 2). Model fluxes were significantly different between littoral and
 372 pelagic zones in Inre and Mellersta Harrsjön (paired t-tests, $p \leq 0.02$), reflecting spatial differences in the
 373 surface water concentration (Table 2). Similar to the chamber fluxes, the air-water concentration
 374 difference ($\Delta[\text{CH}_4]$) explained most of the temporal variability of the modelled emissions; both k_{mod} (Eq.
 375 4) and k_{ch} (Eq. 2) were functions of U_{10} (Fig. 4k) and did not display a distinctive seasonal pattern (Fig. 4i).
 376 Modelled fluxes were lower at higher wind speeds and displayed a cut-off at $U_{10} \geq 6.5 \text{ m s}^{-1}$, similar to
 377 the chamber fluxes, but not at $U_{10} < 2.0 \text{ m s}^{-1}$. The temperature sensitivity of the modelled fluxes ($E_a' =$
 378 $0.97 \pm 0.12 \text{ eV}$, mean \pm 95% CI, $R^2 = 0.94$) did not differ significantly from that of the chamber fluxes.

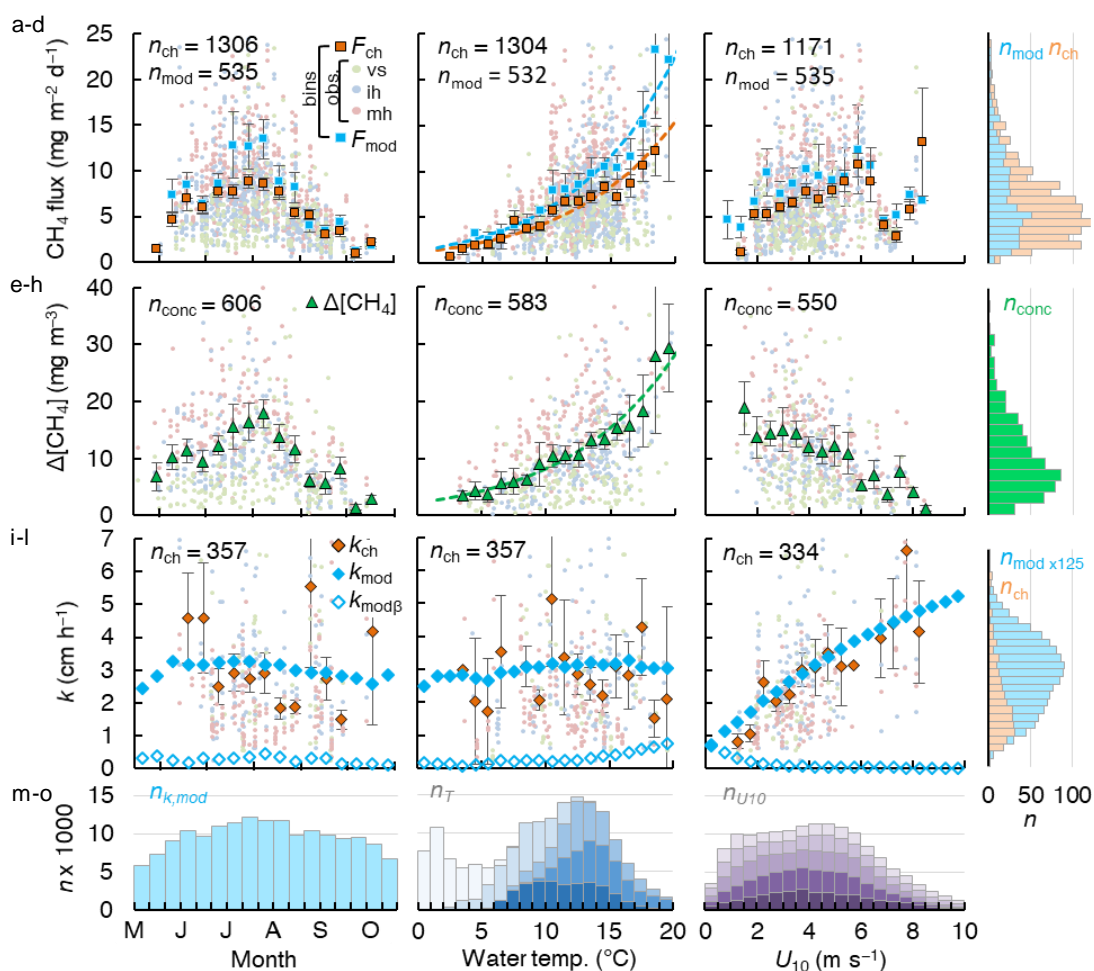
380 **Table 2** – CH_4 fluxes from floating chambers and the surface renewal model, and surface CH_4 concentrations. 2014
 381 was excluded from the model flux means because of a substantial bias in the timing of sample collection.

| Location | Chamber flux ($\text{mg m}^{-2} \text{ d}^{-1}$) | | Modelled flux ($\text{mg m}^{-2} \text{ d}^{-1}$) | | Surface concentration (mg m^{-3}) | |
|----------------------|--|------|---|-----|--|-----|
| | mean \pm 95% CI | n | mean \pm 95% CI | n | mean \pm 95% CI | n |
| Overall | 6.9 ± 0.3 | 1306 | 7.6 ± 0.5 | 501 | 11.9 ± 0.9 | 606 |
| Villasjön | 5.2 ± 0.5 | 249 | 5.3 ± 0.7 | 149 | 8.3 ± 1.1 | 183 |
| Inre Harrsjön | 6.6 ± 0.4 | 532 | 6.9 ± 0.6 | 176 | 10.2 ± 1.0 | 211 |
| Shallow (<2 m) | 6.0 ± 0.6 | 219 | 7.6 ± 0.8 | 113 | 11.1 ± 1.3 | 133 |
| Intermediate (2-4 m) | 7.1 ± 0.6 | 212 | | | | |
| Deep (>4 m) | 6.6 ± 0.8 | 101 | 6.4 ± 0.9 | 63 | 8.6 ± 1.4 | 78 |
| Mellersta Harrsjön | 8.0 ± 0.4 | 525 | 10.4 ± 0.9 | 176 | 16.7 ± 2.0 | 212 |
| Shallow (<2 m) | 8.1 ± 0.6 | 272 | 11.1 ± 1.3 | 113 | 18.2 ± 2.7 | 134 |
| Intermediate (2-4 m) | 7.8 ± 0.7 | 154 | | | | |
| Deep (>4 m) | 8.0 ± 1.0 | 99 | 9.1 ± 1.2 | 63 | 14.1 ± 2.7 | 78 |

382



383
 384
 385
 386
 387
 388
 389
 390
 391
 392
 393
 394
 395
 396
 397
 398
 399
 400
 401
 402
 403
 404
 405
 406
 407
 408
 409
 410
 411
 412
 413
 414
 415
 416
 417



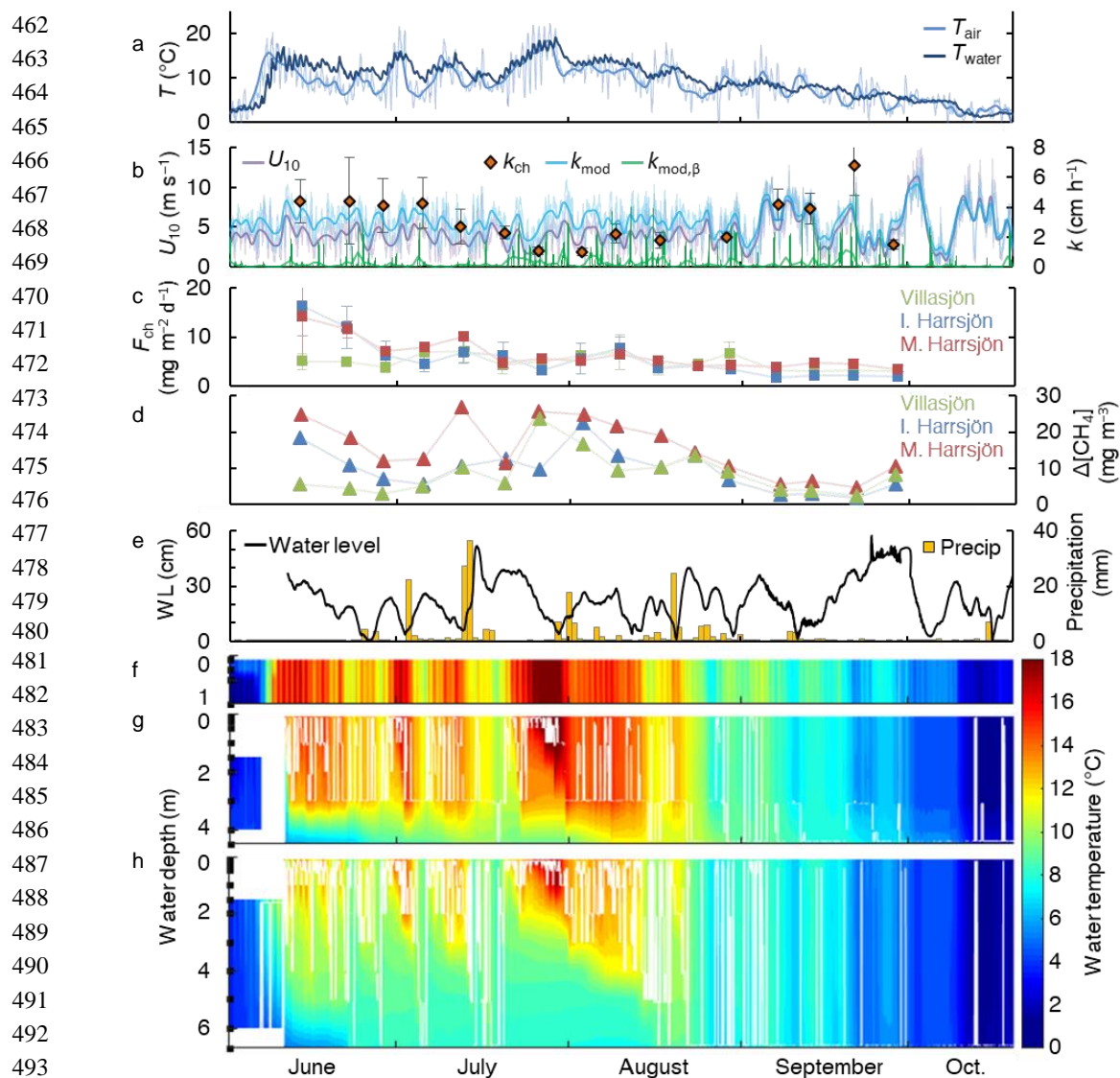
418 **Figure 4** – Scatterplots of the CH₄ flux (a-c), CH₄ air-water concentration difference (e-g) and gas transfer
 419 velocity (i-k) versus time, surface water temperature and wind speed, as well as the histograms of the
 420 aforementioned variables. In each scatter plot binned means are represented by large symbols with
 421 error bars signifying 95% confidence intervals. Bin sizes were 10 days, 1 °C and 0.5 m s⁻¹ for time, surface
 422 water temperature and U₁₀, respectively. Small green, blue and red dots represent individual
 423 measurements in Villasjön, Inre Harrsjön and Mellersta Harrsjön, respectively. Open rhombus symbols in
 424 panels i-k represent the buoyancy component of the gas transfer velocity, closed rhombus symbols
 425 include both the wind-driven and buoyancy-driven components. Dashed lines in panels b and f represent
 426 fitted Arrhenius functions (Eq. 7). Histograms of modelled (light blue) and measured (light orange)
 427 quantities (d,h,l) overlap. Histograms of the surface water temperature (m) and U₁₀ (o) are stacked by
 428 month, from June (darkest shade) to October (lightest shade).



429 3.2 Meteorology and mixing regime

430 The water column of all three lakes was weakly stratified throughout the ice-free season, and the mean
431 diel mixing depths ($d\rho/dz < 0.03 \text{ kg m}^{-3} \text{ m}^{-1}$ (Rueda et al., 2007)) exceeded the lake mean depths (Table
432 3). Figure 5 shows a timeseries of the mixing depth and water temperature in the deeper lakes, along
433 with wind speed, air temperature and precipitation for the ice-free period of 2017. All lakes were
434 polymictic and mixed to the bottom several times during summer (Fig. 5 f-h). Water temperatures in the
435 surface mixed layer were lowest in Mellersta Harrsjön ($9.4 \pm 5.0 \text{ }^\circ\text{C}$), where the mooring was placed next
436 to the stream outlet (Fig. 1), and were higher in Inre Harrsjön ($9.9 \pm 5.5 \text{ }^\circ\text{C}$) and Villasjön ($10.2 \pm 5.3 \text{ }^\circ\text{C}$)
437 (ice-free seasons of 2009–2017, mean \pm SD). In early summer (June, July) deep mixing followed surface
438 cooling and heavy rainfall. Water level maxima and surface temperature minima were observed 2–3 days
439 after rainfall events, for example between 15 and 18 July 2017 (Fig. 5e). Strong nocturnal cooling on 16
440 August 2017 broke up stratification and the lakes remained well-mixed until ice-on (20 October).
441 Increased wind speeds in September and October may have further enhanced mixing. Overall (2009–
442 2018), stratified periods ($z_{\text{mix}} \leq 1 \text{ m}$) were common (29% and 44% of the time in Inre and Mellersta
443 Harrsjön, respectively) but were frequently interrupted by deeper mixing events. Shallow mixing ($z_{\text{mix}} \leq$
444 z_{mean}) occurred on diel timescales. Deep mixing occurred at longer intervals (days-weeks), and more
445 frequently toward the end of the ice-free season (Fig. 5g,h).

446 The gas transfer velocity generally followed the temporal pattern of the wind speed (Fig. 4b). Due to
447 model calibration, the chamber-derived gas transfer velocities (Fig. 4b, orange rhombuses) tracked those
448 computed with the surface renewal model (Fig. 4b, blue line). Discrepancies pointed to a mismatch
449 between 24-hour integrated chamber fluxes and surface concentrations measured at a single point in
450 time. For example, measuring a low surface concentration in the de-gassed water column after a windy
451 period during which the surface flux was high led to an overestimated k_{ch} on 21 September 2017.
452 Contrastingly, k_{ch} was lower than k_{mod} on 3 August 2017 due to elevated surface concentrations and a
453 low chamber flux associated with a warm and stratified period preceding sampling. The mixed layer
454 water temperature exceeded the air temperature by $1.6 \text{ }^\circ\text{C}$ on average (Fig. 5a). The bias was a function
455 of temperatures at night dropping below surface water temperatures, which contributed to negative
456 buoyancy fluxes at night and during cold fronts throughout the ice-free season (Fig 5b, Fig. 4i-k). We
457 computed elevated contributions of the buoyancy flux to the TKE budget during the night and in the
458 warmest months (Fig. 7), but the overall influence of convection on near-surface turbulence was minor.
459 Averaged over all ice-free seasons (2009–2017) the buoyancy flux contributed only 8% to the TKE
460 dissipation rate, but up to 90% during rare, very calm periods ($U_{10} \leq 0.5 \text{ m s}^{-1}$, Fig. 4k) and up to 25% on
461 the warmest days ($T_{\text{surf}} \geq 18 \text{ }^\circ\text{C}$, Fig. 4j).



494 **Figure 5** – Timeseries of air and mixed-layer water temperature (a), wind speed, gas transfer velocity
 495 from the surface renewal model (k_{mod} and its buoyancy component, $k_{\text{mod},\beta}$) and from chamber
 496 observations (k_{ch}) (three-lake mean values, error bars represent 95% confidence intervals) (b), chamber
 497 CH_4 flux (c), air-water CH_4 concentration difference (d), precipitation and changes in water level in
 498 Mellersta Harrsjön (e) and the water temperature in Villasjön (f), Inre Harrsjön (g) and Mellersta Harrsjön
 499 (h) during the ice-free season of 2017 (1 June to 20 October). The white lines in panels e and f represent
 500 the depth of the actively mixing layer. Thin and thick curves in panels a and b represent half-hourly and
 501 daily means, respectively. In panel a only the half-hourly timeseries of T_{water} was plotted.



502 **Table 3** – Lake morphometry, mixing regime and CH₄ residence time. Mean values were calculated over the ice-free
 503 seasons of 2009–2017.

| Lake | Area (ha) | Depth (m) | | Mixed layer depth (m) | | N (cycles h ⁻¹) | | CH ₄ residence time (days) | |
|--------------------|-----------|-----------|-----|-----------------------|-------|-----------------------------|-------|---------------------------------------|----|
| | | mean | max | mean ± SD | n | mean ± SD | n | mean ± SD | n |
| Villasjön | 17.0 | 0.7 | 1.3 | 0.7 ± 0.3 | 66439 | 5.7 ± 8.0 | 59552 | 1.0 ± 0.4 | 72 |
| Inre Harrsjön | 2.3 | 2.0 | 5.2 | 2.5 ± 1.6 | 58362 | 5.2 ± 6.9 | 66757 | 3.4 ± 1.9 | 73 |
| Mellersta Harrsjön | 1.1 | 1.9 | 6.7 | 3.2 ± 2.9 | 62472 | 5.3 ± 9.0 | 61268 | 3.7 ± 1.7 | 72 |

504

505 3.3 CH₄ storage and residence times

506 Residence times of stored CH₄ varied between 12 hours and 7 days and were inversely correlated with
 507 wind speed in all three lakes (OLS: R² ≥ 0.57, Fig. 6). The mean residence time was shortest in the
 508 shallowest lake, and was not significantly different between the two deeper lakes (paired t-test, *p* < 0.01,
 509 Table 3). We did not find a statistically significant linear correlation between the residence time and day
 510 of year or the water temperature. CH₄ storage was greatest in the deeper lakes and displayed patterns
 511 similar to the surface concentrations, increasing in the warmest months with water temperature and
 512 decreasing with wind speed.

513

514

515

516

517

518

519

520

521

522

523

524

525

526

527

528

529

530

531

532

533

534

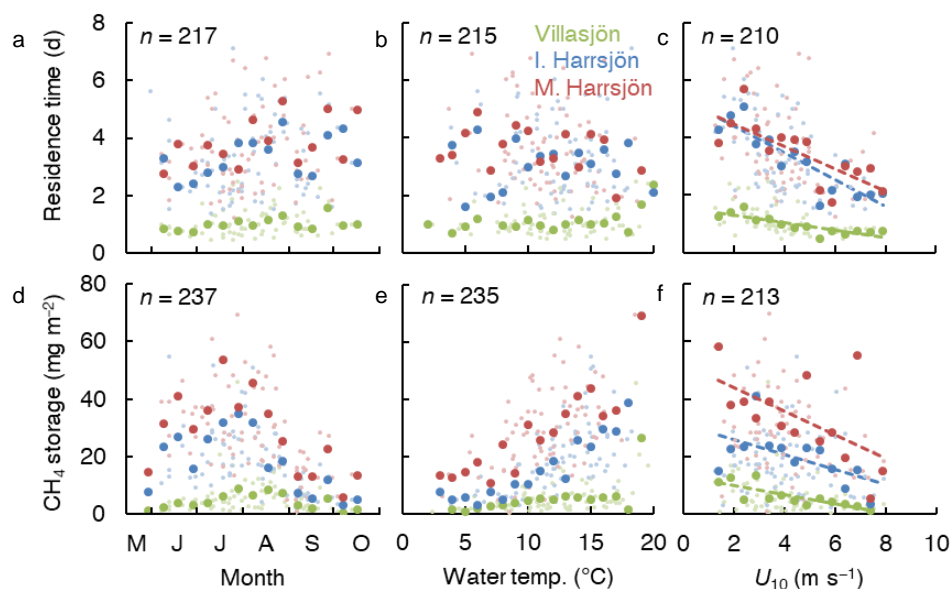
535

536

537

538

539



533 **Figure 6** – Scatterplots of the CH₄ residence time and storage versus time, surface water temperature
 534 and wind speed. Symbol colours represent the different lakes. Large symbols represent binned means,
 535 small symbols represent individual estimates. Bin sizes were 10 days, 1 °C and 0.5 m s⁻¹ for time, water
 536 temperature and U₁₀, respectively. Linear relations of binned quantities and the wind speed were
 537 statistically significant (residence time: *p* ≤ 0.002; storage: *p* ≤ 0.04). The linear regressions of the
 538 residence time onto time of measurement and the surface water temperature were not statistically
 539 significant (*p* = 0.07–0.10).



540 3.4 Variability

541 Chamber fluxes and surface water concentrations differed significantly between lakes (ANOVA, $p <$
 542 0.001 , $n = 287$, $n = 365$). Both quantities were inversely correlated with lake surface area (Table 2). CH_4
 543 concentrations in the stream feeding the Mire ($22.2 \pm 5.1 \text{ mg m}^{-3}$, $n = 29$, mean \pm 95% CI), were
 544 significantly higher than those in the lakes (Table 2) (Lundin et al., 2013). Surface water concentrations
 545 over the deep parts of the deeper lakes ($\geq 2 \text{ m}$ water depth) were lower than those in the shallows (< 2
 546 m) by 21 to 26% for Inre and Mellersta Harrsjön, respectively. However, the diffusive CH_4 flux did not
 547 differ significantly between depth zones in either Inre Harrsjön (ANOVA, $p = 0.27$, $n = 290$) or Mellersta
 548 Harrsjön (ANOVA, $p = 0.90$, $n = 293$), or between zones of high and low CH_4 ebullition in Villasjön (paired
 549 t-test, $p = 0.27$, $n = 89$). This is a contrast with ebullition, for which the highest fluxes were consistently
 550 observed in the shallow lake and littoral areas of the deeper lakes (Jansen et al., 2019; Wik et al., 2013).

551

552 Relations between the flux and its drivers — temperature, wind speed and the surface concentration —
 553 manifested on different timescales (Fig. 7). Over the ice-free season both the CH_4 fluxes and surface
 554 water concentrations tracked changes in the water temperature. The wind speed (U_{10}) showed less
 555 variability over seasonal (CV = 7%, $n = 17$) than over diel timescales (CV = 12%, $n = 24$) and displayed a
 556 clear diurnal maximum. The surface water/sediment temperature varied primarily on a seasonal
 557 timescale (CV = 52%/45%, $n = 17$), and less on diel timescales (CV = 3%/2%, $n = 24$). Similar to the wind
 558 speed the gas transfer velocity varied primarily on diel timescales (Fig. 7), albeit with a lower amplitude,
 559 because $k_{\text{mod}} \propto u^{3/4}$ (Eq. 4). The surface concentration correlated with wind speed and temperature
 560 (Fig. 4f,g), and showed both seasonal and diel variability. On diel timescales $\Delta[\text{CH}_4]$ appeared out of
 561 phase with k_{mod} and peaked just before noon, when the gas transfer velocity reached its maximum value
 562 (Fig. 7b,d). However, binned means of $\Delta[\text{CH}_4]$ were not significantly different at the 95% confidence level
 563 (error bars) and the 1-hour chamber fluxes did not show a clear diel pattern (Fig. 7b).

564

565

566

567

568

569

570

571

572

573

574

575

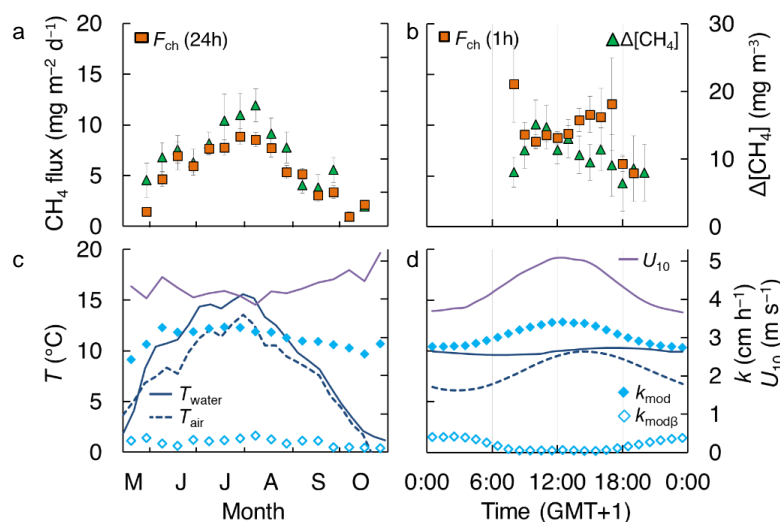
576

577

578

579

580



581 **Figure 7** – Temporal patterns of CH_4 chamber fluxes, concentrations (a,b), gas transfer velocity, air and
 582 surface water temperature and wind speed (c,d). Bin sizes are 10 days (a,c) and 1 hour (b,d). Error bars
 583 represent 95% confidence intervals of the binned means.

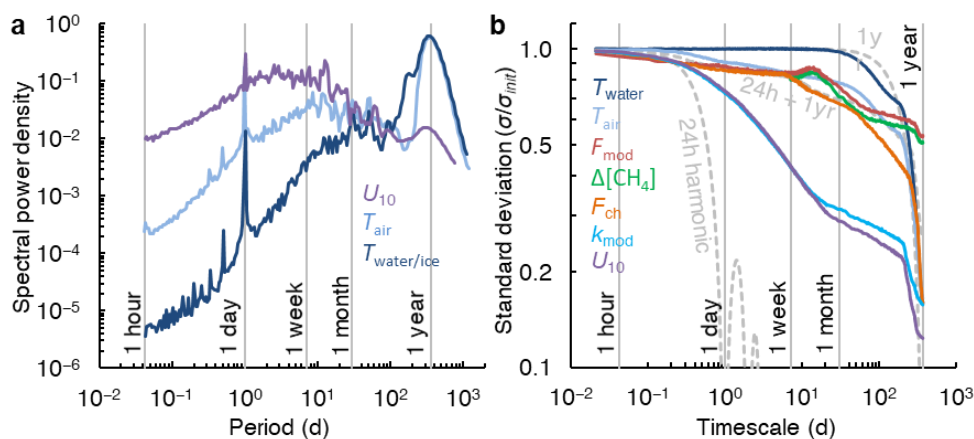


584 **3.5 Timescale analysis**

585 The spectral density plot (Fig. 8a) disentangles dominant timescales of variability of the drivers of the
586 flux. The power spectra of wind speed and temperature peaked at periods of 1 day and 1 year, following
587 well-known diel and annual cycles of insolation and seasonal variations in climate (Baldocchi et al.,
588 2001). For U_{10} , the overall spectral density maximum between 1 day and 1 week corresponds to
589 synoptic-scale weather variability, such as the passage of fronts (MacIntyre et al., 2009). U_{10} and T_{air} also
590 exhibit spectral density peaks at 1–3 weeks, which could be associated with persistent atmospheric
591 blocking typical of the Scandinavian region (Tyrlis and Hoskins, 2008). While the temperature variability
592 was concentrated at annual timescales, the wind speed varied primarily on timescales shorter than
593 about a month.

594

595 The climacogram (Fig. 8b) reveals that the variability of the chamber flux and the gas transfer velocity
596 was enveloped by that of the water temperature and the wind speed, as was the surface concentration
597 difference for timescales < 5 months. The distribution of variability over the different timescales is
598 similar to that shown in the spectral density plot (Fig. 8a). The standard deviation of the water
599 temperature did not change from its initial value ($\sigma/\sigma_{\text{init}} = 1$) until timescales of about 1 month, following
600 the 1 year harmonic. In contrast, most of the variability of the wind speed was concentrated at time
601 scales shorter than 1 month. The variability of the chamber and modelled fluxes first tracked that of the
602 wind speed, but for timescales longer than about 1 month the decrease in variability resembled that of
603 water temperature. The variability of the modelled fluxes followed that of the surface concentration
604 difference rather than the gas transfer velocity. However, the coarse sampling resolution of the fluxes
605 and concentrations may have led to an underestimation of both the variability at <1 week timescales
606 (Fig. 7b) and the value of σ_{init} . Finally, the climacogram shows that k_{mod} retains about 72% of its variability
607 at 24-hour timescales, which justifies our averaging over chamber deployment periods for comparison
608 with k_{ch} and the computation of the model scaling parameter α' (Fig. 3).



609

610 **Figure 8** – Timescale analysis of the diffusive CH_4 flux and its drivers. **a**: Normalized spectral density of
611 whole-year near-continuous timeseries of the air temperature (T_{air}), surface water temperature (0.1–0.5
612 m, $T_{water/ice}$) and the wind speed (U_{10}). **b**: Climacogram of the measured and modelled CH_4 flux (F_{ch} , F_{mod}),
613 the air and surface water temperature (T_{air} , T_{water}), water-air concentration difference ($\Delta[CH_4]$), modelled
614 gas transfer velocity (k_{mod}) and the wind speed (U_{10}) during the ice-free seasons of 2009–2017. Dashed,
615 light-grey curves represent (combinations of) trigonometric functions of mean 0 and amplitude 1 with a
616 specified period. 24h and 1yr harmonic functions were continuous over the dataset period while the 24h
617 + 1yr harmonic was limited to periods when chamber flux data were available.



618 **4. Discussion**

619 **4.1 Magnitude**

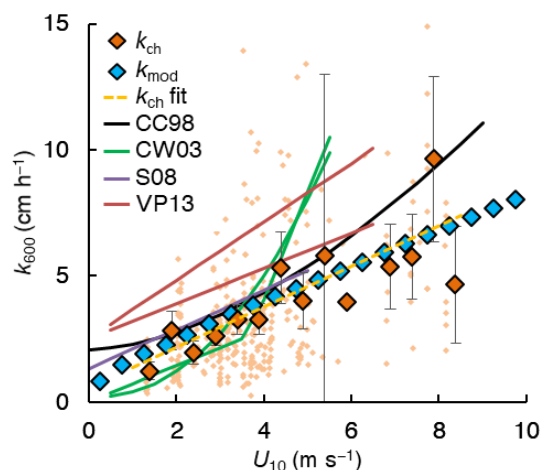
620 Overall, diffusive emissions were lower than the average of postglacial lakes north of 50°N, but within
621 the interquartile range (12.5, 3.0–17.9 mg m⁻² d⁻¹, Wik et al., 2016b). Emissions are also on the lower
622 end of the range for northern lakes of similar size (0.01–0.2 km²) (1–100 mg m⁻² d⁻¹, Wik et al., 2016b).
623 As emissions of the Stordalen lakes do not appear to be limited by substrate quality or quantity (Wik et
624 al., 2018), but strongly depend on temperature (Fig. 4b), the difference is likely because a majority of flux
625 measurements from other postglacial lakes were conducted in the warmer, subarctic boreal zone. Boreal
626 lake CH₄ emissions are generally higher for lakes of similar size: 20–40 mg m⁻² d⁻¹ (binned means), $n = 91$
627 (Rasilo et al., 2015); ~ 12 mg m⁻² d⁻¹, $n = 72$ (Juutinen et al., 2009).

628

629 The gas transfer velocity in the Stordalen lakes was similar to Cole and Caraco (1998) and Crusius and
630 Wanninkhof (2003) at low wind speeds, both of which were based on tracer experiments with sampling
631 over several days, and thus, like our approach, are integrative measures (Fig. 9). At higher winds we
632 obtain lower k -values by nearly a factor of 2 (Table S1). The slope of the linear wind- k_{ch} relation (OLS:
633 0.81 ± 0.21 , slope $\pm 95\%$ CI, dashed yellow line in Fig. 9) was similar to that reported by Soumis et al.
634 (2008) (0.78 for a 0.06 km² lake), who also used a mass balance approach, and Vachon and Prairie (2013)
635 (0.70–1.16 for lakes 0.01–0.15 km²). Part of the difference with literature models was caused by the
636 offset at 0 wind speed, which may stem from a larger contribution of the buoyancy flux (Crill et al., 1988;
637 Read et al., 2012) or from remnant wind shear turbulence (MacIntyre et al., 2018). Another explanation
638 may be the damping of turbulence by near-surface stratification (MacIntyre et al., 2010, 2018), however,
639 such stratification was intermittent in our study (Fig. 5f-h). It may also result from our typically having a
640 stable atmosphere in the day for much of the summer which reduces momentum transfer to the water
641 surface. While our calculations take atmospheric stability into account, work on modelling momentum
642 flux and related drag coefficients under stable atmospheres is ongoing and may lead to lower dissipation
643 rates than we compute (Grachev et al., 2013). Due to the large spread of the chamber-derived gas
644 transfer velocities (small rhombuses, Fig. 9) a power-law exponent to U_{10} ($1.0_{0.0}^{1.8}$; exponent and 95% CI)
645 and thus the nature of the wind- k relation could not be determined with confidence.



646
 647
 648
 649
 650
 651
 652
 653
 654
 655
 656



657 **Figure 9** – Normalized gas transfer velocities (k_{600}) versus the wind speed at 10 m (U_{10}). Binned values
 658 (large rhombuses) and individual observations (small rhombuses) from floating chambers (k_{ch}) and the
 659 surface renewal model (k_{mod} with $\alpha' = 0.24$). Error bars represent 95% confidence intervals of the binned
 660 means. Solid lines represent models from the literature: Cole and Caraco (1998), Crusius and
 661 Wanninkhof (2003) (bilinear and power law models), Soumis et al. (2008) and Vachon and Prairie (2013)
 662 for lake surface areas of 0.01 and 0.15 km². Supplementary Table 1 lists the model equations and
 663 calibration ranges. A linear regression model is shown for the k_{ch} data (dashed yellow line): $k_{600} =$
 664 $0.8_{0.6}^{1.0} \times U_{10} + 0.6_{-0.2}^{+1.3}$ (sub- and superscripts denote 95% confidence intervals), with $R^2 = 0.20$ for
 665 individual chamber values (small orange rhombuses) and $R^2 = 0.64$ for the binned means (large orange
 666 rhombuses).



667 **4.2 Drivers of the flux**

668 The Arrhenius-type relation of CH₄ fluxes and concentrations (Fig. 4b,f) together with short CH₄ residence
669 times (Fig. 6) suggest that emissions from the Stordalen lakes were strongly coupled to sediment
670 production through efficient redistribution of dissolved CH₄. High CH₄ concentrations in the stream
671 suggest that terrestrial inputs of CH₄ may have elevated emissions in Mellersta Harrsjön (Lundin et al.,
672 2013; Paytan et al., 2015). Similarly, terrestrial inputs of nutrients may have indirectly enhanced
673 emissions in the littoral zones by supporting production of autochthonous organic substrates (Davidson
674 et al., 2018; Rantala et al., 2016). However, although the Mire exports substantial quantities of DOC and
675 presumably CH₄ from the water-logged fens to the lakes (Olefeldt and Roulet, 2012), after cold and rainy
676 periods we observed either a decrease in $\Delta[\text{CH}_4]$ (13–19 July 2017, Fig. 5) or no significant change (3–6
677 July and 21–27 August 2017, Fig. 5). It remains unclear whether such reduced storage resulted from
678 lower methanogenesis rates, convection-induced degassing or lake water displacement by surface
679 runoff.

680
681 Turbulent transfer was dominated by wind shear in the Stordalen lakes. We computed a minor
682 contribution (~8%) of the buoyancy-controlled fraction of k ($k_{600,\beta} = 0.3 \text{ cm h}^{-1}$) (ice-free season mean,
683 2009–2017). Our results differ from that in Read et al. (2012) who expect a dominant role of convection
684 to k in small lakes. The difference here results from low values of sensible and latent heat fluxes due to
685 colder temperatures during summer such that net long wave radiation was often less than 50 W m^{-2} .
686 Lakes in warmer regions with lower humidity and clearer skies and low wind speeds particularly at night
687 will have a larger contribution of buoyancy flux to the gas transfer coefficient (MacIntyre and Melack,
688 2009). The contribution of convection also depends on the wind-sheltering properties of the landscape
689 surrounding the lake (Kankaala et al., 2013; Markfort et al., 2010). Depending on the turbulence
690 environment the buoyancy flux is thus weighed differently in parameterizations of ϵ (Heiskanen et al.,
691 2014; Tedford et al., 2014) and in wind-based models (offsets at $U_{10} = 0$ in Fig. 9), contributing to
692 significant differences between model realizations of k (Dugan et al., 2016; Erkkilä et al., 2018; Schilder
693 et al., 2016). We expect our results to be representative of small, wind-exposed lakes in cold
694 environments.

695
696 **4.3 Storage and stability**

697 The lake mixing regime can modulate flux-temperature relationships by periodically decoupling
698 production from emission rates (e.g. Yvon-Durocher et al., 2014). Enhanced accumulation during periods
699 of stratification may have contributed to concentration and storage maxima in July and August (Fig. 4e,
700 6d). However, as the CH₄ residence time was invariant over the season and with temperature (Fig. 6a,b),
701 the storage-temperature relation (Fig. 6e) likely reflects rate changes in sediment methanogenesis rather
702 than inhibited mixing. For example, the highest CH₄ concentrations in our dataset ($59.1 \pm 26.4 \text{ mg m}^{-3}$, n
703 = 37) were measured during a period with exceptionally high surface water temperatures ($T_{\text{water}} = 18.5 \pm$
704 $3.6 \text{ }^\circ\text{C}$) that lasted from 23 June to 30 July 2014. Emissions during this period comprised 29%–56%
705 (depending on lake) of the 2014 ice-free diffusive flux, while the peak quantity of accumulated CH₄ was
706 <5%. Two mechanisms may explain the lack of CH₄ accumulation. First, stratification was frequently
707 disrupted by vertical mixing (Fig. 5g-h) and concurrent hypolimnetic CH₄ concentrations were not
708 significantly different from (Inre Harrsjön, 2010–2017, paired t-test, $p = 0.12$, $n = 32$) or lower than



709 (Mellersta Harrsjön, 2010–2017, paired t-test, $p < 0.01$, $n = 35$) those in the surface mixed layer. Second,
710 stratification often was not strong enough to affect gas transfer velocities ($N > 25$ during $< 17\%$ of this
711 period). Even when assuming ϵ was suppressed by an order of magnitude for $N > 25$ and by two orders of
712 magnitude for $N > 40$ (MacIntyre et al., 2018), k_{mod} was only slightly lower (2.8 cm h^{-1}) than the multi-year
713 mean (3.0 cm h^{-1}). Thus, in weakly stratified, polymictic lakes, the temperature sensitivity of diffusive CH_4
714 emissions may be observed without significant modulation by stratification.

715
716 The water-air concentration difference acted as a negative feedback that maintained a quasi steady state
717 between CH_4 production and removal processes throughout the ice-free season. In other words, higher
718 temperatures led to elevated CH_4 concentrations (Fig. 4f) which in turn increased emission rates (Eq. 1,
719 Fig. 4b). However, in contrast to the temperature-binned fluxes, when binned by wind speed high
720 emission rates were associated with low concentrations (Fig. 4c,g). In this way the $\Delta[\text{CH}_4]$ feedback
721 limited the increase of the emission rate with the gas transfer velocity. In all three lakes CH_4 residence
722 times were inversely proportional to the wind speed (Fig. 6c), indicating an imbalance between
723 production and removal processes. We hypothesize that the imbalance exists because the variability of
724 wind speed peaked on shorter timescales than that of the water temperature (Fig. 8a). Changes in wind
725 shear periodically pushed the system out of production-emission equilibrium, allowing for transient
726 degassing and accumulation of dissolved CH_4 . The temporal variability of dissolved gas concentrations is
727 likely higher in wind-exposed systems with limited buffer capacity (Natchimuthu et al., 2016, 2017), and
728 should be taken into account when applying gas transfer models to small lakes and ponds.

729
730 Rapid degassing occurred at $U_{10} > 6.5 \text{ m s}^{-1}$ (Fig. 4c, mean wind speed during chamber deployments). Gas
731 fluxes at high wind speeds may have been enhanced by the kinetic action of breaking waves (Terray et
732 al., 1996) or through microbubble-mediated transfer. Wave breaking was observed on the Stordalen
733 lakes at wind speeds $\geq 7 \text{ m s}^{-1}$. Microbubbles of atmospheric gas (diameter $< 1 \text{ mm}$) can form due to
734 photosynthesis, rain or wave breaking (Woolf and Thorpe, 1991) and remain entrained for several days
735 (Turner, 1961). Due to their relatively large surface area they quickly equilibrate with sparingly soluble
736 gases in the water column, providing an efficient emission pathway to the atmosphere when the bubbles
737 rise to the surface (Merlivat and Memery, 1983). In inland waters microbubble emissions of CH_4 have
738 only been indirectly inferred from differences in CO_2 and CH_4 gas transfer velocities (McGinnis et al.,
739 2015; Prairie and del Giorgio, 2013), and more work is needed to evaluate their significance in relatively
740 sheltered systems.

742 4.4 Timescales of variability

743 Overall, the short-term variability of the flux due to wind speed was similar to the long-term variability
744 due to temperature (ranges of the binned means, Fig. 4a-c). The diel patterns in the mixing depth (Fig. 5)
745 and the gas transfer velocity (Fig. 7d) and daytime variation of the surface concentration (Fig. 7b) were
746 indicative of daily storage-and-release cycles, resulting in a model flux difference of about $5 \text{ mg m}^{-2} \text{ d}^{-1}$
747 between morning and afternoon; about half the mean seasonal range (Fig. 7a). Diel variability of lake
748 methane fluxes has been observed at Villasjön (eddy covariance, Jammot et al., 2017) and elsewhere
749 (Bastviken et al., 2004, 2010; Crill et al., 1988; Erkkilä et al., 2018; Eugster et al., 2011; Hamilton et al.,
750 1994; Podgrajsek et al., 2014b). Similarly, diel patterns in the gas transfer velocity have been observed



751 with the eddy covariance technique (Podgrajsek et al., 2015) and in model studies (Erkkilä et al., 2018).
752 Apparent offsets between the diurnal peaks of the flux, surface concentrations and drivers (Fig 7b,d)
753 have been noted previously (Koebsch et al., 2015), but have yet to be explained. Continuous eddy
754 covariance measurements in lakes where the dominant emission pathway is turbulence-driven diffusion
755 could help characterize flux variability on short timescales (e.g. Bartosiewicz et al., 2015).

756
757 The CH₄ residence times (1–3 days) were not much longer than the diel timescale of vertical mixing (Fig.
758 5g,h). As a result, horizontal concentration gradients developed in the deeper lakes (Table 2). The $23 \pm$
759 11% concentration difference between depth zones in the deeper lakes (mean \pm 95%) fits transport
760 model predictions of DeSontro et al. (2017) for small lakes (< 1 km²) that highlight the role of outgassing
761 and oxidation during transport from production zones in the shallow littoral zones or the deeper
762 sediments (Hofmann, 2013). Concentration gradients may also have been caused by physical processes,
763 such as upwelling due to thermocline tilting (Heiskanen et al., 2014). Higher resolution measurements,
764 for example with automated equilibration systems (Erkkilä et al., 2018; Natchimuthu et al., 2016), are
765 needed to assess how much of the spatial and diel patterns of the CH₄ concentration can be explained by
766 physical drivers such as gas transfer and mixed layer deepening (Eugster et al., 2003; Vachon et al.,
767 2019), or by biological processes such as methanogenesis and microbial oxidation (Ford et al., 2002).

768
769 The distinct spectral peaks of U₁₀ and temperature (Fig. 8) suggest that flux dependencies on these
770 parameters (Fig. 4b,c) acted on different timescales. This has implications for the choice of models or
771 proxies of the flux in predictive analyses. For polymictic lakes and a climatology similar to that of the
772 Stordalen Mire (Malmer et al., 2005), temperature-based proxies (e.g. Thornton et al., 2015) would
773 resolve most of the variability of the ice-free diffusive CH₄ flux at timescales longer than a month.
774 Advanced gas transfer models that account for atmospheric stability and rapid variations in wind shear
775 are necessary to resolve the flux variability at timescales shorter than about a month. However, gas
776 transfer models can only deliver accurate fluxes if they are combined with measurements that capture
777 the full spatiotemporal variability of the surface concentration (Erkkilä et al., 2018; Hofmann, 2013;
778 Natchimuthu et al., 2016; Schilder et al., 2016). The short CH₄ residence times and diel pattern of $\Delta[\text{CH}_4]$
779 suggest that weekly sampling did not capture the full temporal variability of the surface concentrations.
780 Especially after episodes of high wind speeds and lake degassing (Fig. 4c,g), concentrations may not have
781 been representative of the 24-hour chamber deployment period.



782 4.6 Model-chamber comparison

783 Comparing gas transfer velocities from the floating chambers and the surface renewal model we find a
784 scaling parameter value (α' in Eq. 4) of approximately 0.24 (Fig. 3). Its theoretical value (α) is $\sqrt{2/15} \cong$
785 0.37 (Katul et al., 2018) but empirically derived values (α') can vary between 0.1 and 0.7 over the range
786 of moderate to high dissipation rates computed for the Stordalen lakes (Eq. 5: $\varepsilon = 10^{-7}$ – 10^{-5} m² s⁻³)
787 (Esters et al., 2017; Wang et al., 2015 and references therein), when ε is measured directly with acoustic
788 Doppler- or particle image velocimetry and compared with independent estimates of k using chambers
789 (Gålfalk et al., 2013; Tokoro et al., 2008; Vachon et al., 2010; Wang et al., 2015), eddy covariance
790 observations (Heiskanen et al., 2014) or the gradient flux technique (Zappa et al., 2007) and a sparingly
791 soluble tracer, such as CO₂ or SF₆. Recent studies report a reasonable agreement between measured and
792 modeled lake CO₂ fluxes if Eq. 4 and Eq. 5 are used with a multi-study mean α' of 0.5 (Bartosiewicz et al.,
793 2015; Czirkowsky et al., 2018; Erkkilä et al., 2018; Mammarella et al., 2015). While there is evidence for
794 similar agreement for CH₄ with $\alpha' = 0.5$ (Erkkilä et al., 2018), this approach may exceed chamber-derived
795 emissions by a factor of 2 (Bartosiewicz et al., 2015) – i.e. closer to our scaling parameter value of 0.24.
796

797 Because the physical drivers of gas exchange have been accounted for in the formulation of k_{mod} ,
798 chemical or biological factors that do not affect turbulence in the actively mixed layer but can limit
799 surface exchange could be responsible for the observed variability in α' . In most freshwater systems a
800 significant fraction of CH₄ is removed through microbial oxidation at the sediment surface and in the
801 water column (Bastviken et al., 2002). The Stordalen lakes remained oxygenated throughout the ice-free
802 season and CH₄ stable isotopes indicate that between 24% (Villasjön) and 60% (Inre and Mellersta
803 Harrsjön) of CH₄ in the water column was oxidized (Jansen et al., 2019). This may explain not only the
804 low scaling parameter value compared to those found with other tracers, but also why α' was higher in
805 Villasjön (0.31, $n = 67$) than in the deeper lakes (0.17–0.25, $n = 267$). However, more work is needed to
806 establish how the oxidation effect partitioned between CH₄ reservoirs in the water column, where it
807 would affect surface emissions, and the sediment. Other biogenic factors may also have impacted gas
808 transfer, such as organic surface slicks in the 10–100 μm diffusive sublayer (Tokoro et al., 2008).
809 Additionally, the wind speed may have been lower over the lakes than on the Mire due to the slight
810 elevation (<1 m) of the surrounding peatland hummocks and the wind-sheltering effect of tall shrubs
811 (*Betula nana* L, Malmer et al., 2005) on the shores of the deeper lakes (Fig. 1) (Markfort et al., 2010).
812

813 4.7 Omitted fluxes?

814 We investigated whether our chamber measurements may have missed high-quantity release from
815 storage (Podgrajsek et al., 2014a). In stratified lakes mixed layer deepening can bring up accumulated
816 gas, resulting in elevated surface fluxes, for example due to night time convection (Eugster et al., 2003),
817 during autumn overturns (Encinas Fernández et al., 2014; Juutinen et al., 2009; Laurion et al., 2010;
818 López Bellido et al., 2009) or rain events (Bartosiewicz et al., 2015; Ojala et al., 2011). Here
819 however, >80% of the lakes' volume mixed on diel timescales and we did not observe substantial CH₄
820 accumulation over summer. Indeed, CH₄ concentrations within the 0.1–1 m surface layer of the deeper
821 lakes (Table 2) were not significantly different from those at greater depth (Inre Harrsjön: 12.2 ± 2.7 mg
822 m⁻³, $n = 292$; Mellersta Harrsjön: 17.7 ± 4.9 mg m⁻³, $n = 405$; means \pm 95% CI). It is therefore unlikely that
823 our chamber fluxes omitted emissions from hypolimnetic storage.



824 **5. Summary and conclusions**

825 In this study we combined a unique, multi-year dataset with a modelling approach to better understand
826 environmental controls on turbulence-driven diffusion-limited CH₄ emissions from small, shallow lakes.
827 Floating chambers estimated the seasonal mean flux at 6.9 mg m⁻² d⁻¹ and illustrated how the flux
828 depended on temperature and wind speed. Wind shear controlled the gas transfer velocity while
829 thermal convection and release from storage were minor drivers of the flux. CH₄ fluxes and surface
830 concentrations fitted an Arrhenius-type temperature function ($E_a' = 0.88\text{--}0.97$ eV), suggesting that
831 emissions were strongly coupled to rates of methanogenesis in the sediment. However, temperature
832 was only an accurate proxy of the flux on averaging timescales longer than a month. On shorter
833 timescales wind-induced variability in the gas transfer velocity, mixed layer depth, and storage
834 decoupled production from emission rates. Transient stratification allowed for periodic CH₄
835 accumulation and resulted in an inverse relationship between wind speed and surface concentrations. In
836 this way, the air-water concentration difference acted as a negative feedback to emissions and
837 prevented complete degassing of the lakes, except at high wind speeds ($U_{10} \geq 6.5$ m s⁻¹).

838
839 Freshwater flux studies are increasingly focused on understanding mechanisms and developing proxies
840 for use in upscaling efforts and process-based models. Our results show that the timescale of driver
841 variability can inform the frequency of field measurements to yield representative datasets.
842 Observations that capture the spatiotemporal variability of dissolved gas concentrations could help
843 realize the potential of advanced gas transfer models to disentangle biogeochemical and physical flux
844 drivers at half-hourly to interannual timescales. Linking model and field measurement approaches could
845 uncover non-linear feedbacks, such as shallow lake degassing at high wind speeds, quantify biases
846 associated with measurement timing and location, and constrain the applicability timescale of novel
847 emission proxies.



848 **6. Data availability**

849 Data are available at www.bolin.su.se/data/.

850

851 **7. Author contribution**

852 JJ, MW and PC designed the study. Fieldwork and laboratory measurements were guided by JJ, JS and
853 MW. SM and AC developed the surface renewal model code. JJ performed the analyses and prepared the
854 manuscript with contributions from BT and SM.

855

856 **8. Competing interests**

857 The authors declare that they have no conflict of interest.

858

859 **9. Acknowledgements**

860 This work was funded by the Swedish Research Council (VR) with grants to P. Crill (#2007-4547 and
861 #2013-5562) and by the U.S. National Science Foundation with Arctic Natural Sciences Grants #1204267
862 and #1737411 to S. MacIntyre. The collection of ICOS data was funded by the Swedish Research Council
863 (#2015-06020). We thank the McGill University researchers (David Olefeldt, Silvie Harder and Nigel
864 Roulet) for the data they provided from the carbon flux tower that was supported by the Natural Science
865 and Engineering Research Council of Canada (# NSERC RGPIN-2017-04059). We are grateful to D.
866 Bastviken for validating our implementation of the chamber headspace equilibration model. We thank
867 the staff at the Abisko Scientific Research Station (ANS) for logistic and technical support. Noah Jansen
868 created the schematic of the floating chamber pair. We thank Carmody McCalley, Christoffer
869 Hemmingsson, Emily Pickering-Pedersen, Erik Wik, Hanna Axén, Hedvig Öste, Jacqueline Amante, Jenny
870 Gålling, Jóhannes West, Kaitlyn Steele, Kim Jäderstrand, Lina Hansson, Lise Johnsson, Livija Ginters,
871 Mathilda Nyzell, Niklas Rakos, Oscar Bergkvist, Robert Holden, Tyler Logan and Ulf Swendsén for their
872 help in the field.

873



874 **10. References**

- 875 Baldocchi, D., Falge, E. and Wilson, K.: A spectral analysis of biosphere–atmosphere trace gas flux
876 densities and meteorological variables across hour to multi-year time scales, *Agric. For. Meteorol.*,
877 107(1), 1–27, doi:10.1016/S0168-1923(00)00228-8, 2001.
- 878 Bartosiewicz, M., Laurion, I. and MacIntyre, S.: Greenhouse gas emission and storage in a small shallow
879 lake, *Hydrobiologia*, 757(1), 101–115, doi:10.1007/s10750-015-2240-2, 2015.
- 880 Bastviken, D., Ejlertsson, J. and Tranvik, L.: Measurement of Methane Oxidation in Lakes: A Comparison
881 of Methods, *Environ. Sci. Technol.*, 36(15), 3354–3361, doi:10.1021/es010311p, 2002.
- 882 Bastviken, D., Cole, J., Pace, M. and Tranvik, L.: Methane emissions from lakes: Dependence of lake
883 characteristics, two regional assessments, and a global estimate, *Global Biogeochem. Cycles*, 18(4),
884 doi:10.1029/2004GB002238, 2004.
- 885 Bastviken, D., Santoro, A. L., Marotta, H., Pinho, L. Q., Calheiros, D. F., Crill, P. and Enrich-Prast, A.:
886 Methane Emissions from Pantanal, South America, during the Low Water Season: Toward More
887 Comprehensive Sampling, *Environ. Sci. Technol.*, 44(14), 5450–5455, doi:10.1021/es1005048, 2010.
- 888 Bastviken, D., Tranvik, L. J., Downing, J. A., Crill, P. M. and Enrich-Prast, A.: Freshwater Methane
889 Emissions Offset the Continental Carbon Sink, *Science* (80-.), 331(6013), 50–50,
890 doi:10.1126/science.1196808, 2011.
- 891 Borrel, G., Jézéquel, D., Biderre-Petit, C., Morel-Desrosiers, N., Morel, J.-P., Peyret, P., Fonty, G. and
892 Lehours, A.-C.: Production and consumption of methane in freshwater lake ecosystems, *Res. Microbiol.*,
893 162(9), 832–847, doi:10.1016/j.resmic.2011.06.004, 2011.
- 894 Cole, J. J. and Caraco, N. F.: Atmospheric exchange of carbon dioxide in a low-wind oligotrophic lake
895 measured by the addition of SF₆, *Limnol. Oceanogr.*, 43(4), 647–656, doi:10.4319/lo.1998.43.4.0647,
896 1998.
- 897 Cole, J. J., Prairie, Y. T., Caraco, N. F., McDowell, W. H., Tranvik, L. J., Striegl, R. G., Duarte, C. M.,
898 Kortelainen, P., Downing, J. A., Middelburg, J. J. and Melack, J.: Plumbing the Global Carbon Cycle:
899 Integrating Inland Waters into the Terrestrial Carbon Budget, *Ecosystems*, 10(1), 172–185,
900 doi:10.1007/s10021-006-9013-8, 2007.
- 901 Crill, P. M., Bartlett, K. B., Wilson, J. O., Sebach, D. I., Harriss, R. C., Melack, J. M., MacIntyre, S., Lesack,
902 L. and Smith-Morrill, L.: Tropospheric methane from an Amazonian floodplain lake, *J. Geophys. Res.*,
903 93(D2), 1564, doi:10.1029/JD093iD02p01564, 1988.
- 904 Crusius, J. and Wanninkhof, R.: Gas transfer velocities measured at low wind speed over a lake, *Limnol.*
905 *Oceanogr.*, 48(3), 1010–1017, doi:10.4319/lo.2003.48.3.1010, 2003.
- 906 Csanady, G. T.: *Air-Sea Interaction - Laws and Mechanisms*, Cambridge University Press., 2001.
- 907 Czikowsky, M. J., MacIntyre, S., Tedford, E. W., Vidal, J. and Miller, S. D.: Effects of Wind and Buoyancy on
908 Carbon Dioxide Distribution and Air-Water Flux of a Stratified Temperate Lake, *J. Geophys. Res.*
909 *Biogeosciences*, 123(8), 2305–2322, doi:10.1029/2017JG004209, 2018.
- 910 Davidson, T. A., Audet, J., Jeppesen, E., Landkildehus, F., Lauridsen, T. L., Søndergaard, M. and Syväranta,
911 J.: Synergy between nutrients and warming enhances methane ebullition from experimental lakes, *Nat.*
912 *Clim. Chang.*, 8(2), 156–160, doi:10.1038/s41558-017-0063-z, 2018.



- 913 DelSontro, T., Boutet, L., St-Pierre, A., del Giorgio, P. A. and Prairie, Y. T.: Methane ebullition and
914 diffusion from northern ponds and lakes regulated by the interaction between temperature and system
915 productivity, *Limnol. Oceanogr.*, 61(S1), S62–S77, doi:10.1002/lno.10335, 2016.
- 916 DelSontro, T., del Giorgio, P. A. and Prairie, Y. T.: No Longer a Paradox: The Interaction Between Physical
917 Transport and Biological Processes Explains the Spatial Distribution of Surface Water Methane Within
918 and Across Lakes, *Ecosystems*, 1–15, doi:10.1007/s10021-017-0205-1, 2017.
- 919 DelSontro, T., Beaulieu, J. J. and Downing, J. A.: Greenhouse gas emissions from lakes and
920 impoundments: Upscaling in the face of global change, *Limnol. Oceanogr. Lett.*, doi:10.1002/lol2.10073,
921 2018.
- 922 Dimitriadis, P. and Koutsoyiannis, D.: Climacogram versus autocovariance and power spectrum in
923 stochastic modelling for Markovian and Hurst–Kolmogorov processes, *Stoch. Environ. Res. Risk Assess.*,
924 29(6), 1649–1669, doi:10.1007/s00477-015-1023-7, 2015.
- 925 Duc, N. T., Crill, P. and Bastviken, D.: Implications of temperature and sediment characteristics on
926 methane formation and oxidation in lake sediments, *Biogeochemistry*, 100(1–3), 185–196,
927 doi:10.1007/s10533-010-9415-8, 2010.
- 928 Dugan, H. A., Woolway, R. I., Santoso, A. B., Corman, J. R., Jaimes, A., Nodine, E. R., Patil, V. P., Zwart, J.
929 A., Brentrup, J. A., Hetherington, A. L., Oliver, S. K., Read, J. S., Winters, K. M., Hanson, P. C., Read, E. K.,
930 Winslow, L. A. and Weathers, K. C.: Consequences of gas flux model choice on the interpretation of
931 metabolic balance across 15 lakes, *Int. Waters*, 6(4), 581–592, doi:10.1080/IW-6.4.836, 2016.
- 932 Encinas Fernández, J., Peeters, F. and Hofmann, H.: Importance of the Autumn Overturn and Anoxic
933 Conditions in the Hypolimnion for the Annual Methane Emissions from a Temperate Lake, *Environ. Sci.*
934 *Technol.*, 48(13), 7297–7304, doi:10.1021/es4056164, 2014.
- 935 Erkkilä, K.-M., Ojala, A., Bastviken, D., Biermann, T., Heiskanen, J. J., Lindroth, A., Peltola, O., Rantakari,
936 M., Vesala, T. and Mammarella, I.: Methane and carbon dioxide fluxes over a lake: comparison between
937 eddy covariance, floating chambers and boundary layer method, *Biogeosciences*, 15(2), 429–445,
938 doi:10.5194/bg-15-429-2018, 2018.
- 939 Esters, L., Landwehr, S., Sutherland, G., Bell, T. G., Christensen, K. H., Saltzman, E. S., Miller, S. D. and
940 Ward, B.: Parameterizing air-sea gas transfer velocity with dissipation, *J. Geophys. Res. Ocean.*, 122(4),
941 3041–3056, doi:10.1002/2016JC012088, 2017.
- 942 Eugster, W., Kling, G., Jonas, T., McFadden, J. P., Wüest, A., MacIntyre, S. and Chapin III, F. S.: CO₂
943 exchange between air and water in an Arctic Alaskan and midlatitude Swiss lake: Importance of
944 convective mixing, *J. Geophys. Res. Atmos.*, 108(D12), doi:10.1029/2002JD002653, 2003.
- 945 Eugster, W., DelSontro, T. and Sobek, S.: Eddy covariance flux measurements confirm extreme CH₄
946 emissions from a Swiss hydropower reservoir and resolve their short-term variability, *Biogeosciences*,
947 8(9), 2815–2831, doi:10.5194/bg-8-2815-2011, 2011.
- 948 Fang, X. and Stefan, H. G.: Dynamics of heat exchange between sediment and water in a lake, *Water*
949 *Resour. Res.*, 32(6), 1719–1727, doi:10.1029/96WR00274, 1996.
- 950 Ford, P. W., Boon, P. I. and Lee, K.: Methane and oxygen dynamics in a shallow floodplain lake: The
951 significance of periodic stratification, *Hydrobiologia*, 485, 97–110, doi:10.1023/A:102137953, 2002.
- 952 Gålfalk, M., Bastviken, D., Fredriksson, S. and Arneborg, L.: Determination of the piston velocity for



- 953 water-air interfaces using flux chambers, acoustic Doppler velocimetry, and IR imaging of the water
954 surface, *J. Geophys. Res. Biogeosciences*, 118(2), 770–782, doi:10.1002/jgrg.20064, 2013.
- 955 Grachev, A. A., Andreas, E. L., Fairall, C. W., Guest, P. S. and Persson, P. O. G.: The Critical Richardson
956 Number and Limits of Applicability of Local Similarity Theory in the Stable Boundary Layer, *Boundary-
957 Layer Meteorol.*, 147(1), 51–82, doi:10.1007/s10546-012-9771-0, 2013.
- 958 Hamilton, J. D., Kelly, C. a, Rudd, J. W. M., Hesslein, R. H. and Roulet, N. T.: Flux to the atmosphere of CH₄
959 and CO₂ from wetland ponds on the Hudson Bay lowlands (HBLs), *J. Geophys. Res.*, 99(D1), 1495,
960 doi:10.1029/93JD03020, 1994.
- 961 Hammer, Ø., Harper, D. A. T. and Ryan, P. D.: Past: Paleontological statistics software package for
962 education and data analysis, *Palaeontol. Electron.*, 4(1) [online] Available from:
963 <https://folk.uio.no/ohammer/past/>, 2001.
- 964 Hamming, R. W.: *Digital Filters*, Dover publications, Dover, New York., 1989.
- 965 Heiskanen, J. J., Mammarella, I., Haapanala, S., Pumpanen, J., Vesala, T., MacIntyre, S. and Ojala, A.:
966 Effects of cooling and internal wave motions on gas transfer coefficients in a boreal lake, *Tellus B Chem.
967 Phys. Meteorol.*, 66(1), 22827, doi:10.3402/tellusb.v66.22827, 2014.
- 968 Hofmann, H.: Spatiotemporal distribution patterns of dissolved methane in lakes: How accurate are the
969 current estimations of the diffusive flux path?, *Geophys. Res. Lett.*, 40(11), 2779–2784,
970 doi:10.1002/grl.50453, 2013.
- 971 Holgerson, M. A. and Raymond, P. A.: Large contribution to inland water CO₂ and CH₄ emissions from
972 very small ponds, *Nat. Geosci.*, 9(3), 222–226, doi:10.1038/ngeo2654, 2016.
- 973 Idso, S. B. and Gilbert, R. G.: On the Universality of the Poole and Atkins Secchi Disk-Light Extinction
974 Equation, *J. Appl. Ecol.*, 11(1), 399, doi:10.2307/2402029, 1974.
- 975 Imberger, J.: The diurnal mixed layer, *Limnol. Oceanogr.*, 30(4), 737–770, doi:10.4319/lo.1985.30.4.0737,
976 1985.
- 977 Jähne, B., Heinz, G. and Dietrich, W.: Measurement of the diffusion coefficients of sparingly soluble gases
978 in water, *J. Geophys. Res.*, 92(C10), 10767, doi:10.1029/JC092iC10p10767, 1987.
- 979 Jammet, M., Crill, P., Dengel, S. and Friborg, T.: Large methane emissions from a subarctic lake during
980 spring thaw: Mechanisms and landscape significance, *J. Geophys. Res. Biogeosciences*, 120(11), 2289–
981 2305, doi:10.1002/2015JG003137, 2015.
- 982 Jammet, M., Dengel, S., Kettner, E., Parmentier, F.-J. W., Wik, M., Crill, P. and Friborg, T.: Year-round CH₄
983 and CO₂ flux dynamics in two contrasting freshwater ecosystems of the subarctic, *Biogeosciences*,
984 14(22), 5189–5216, doi:10.5194/bg-14-5189-2017, 2017.
- 985 Jansen, J., Thornton, B. F., Jammet, M. M., Wik, M., Cortés, A., Friborg, T., MacIntyre, S. and Crill, P. M.:
986 Climate-Sensitive Controls on Large Spring Emissions of CH₄ and CO₂ From Northern Lakes, *J. Geophys.
987 Res. Biogeosciences*, 2019JG005094, doi:10.1029/2019JG005094, 2019.
- 988 Jellison, R. and Melack, J. M.: Meromixis in hypersaline Mono Lake, California. 1. Stratification and
989 vertical mixing during the onset, persistence, and breakdown of meromixis, *Limnol. Oceanogr.*, 38(5),
990 1008–1019, doi:10.4319/lo.1993.38.5.1008, 1993.
- 991 Juutinen, S., Rantakari, M., Kortelainen, P., Huttunen, J. T., Larmola, T., Alm, J., Silvola, J. and



- 992 Martikainen, P. J.: Methane dynamics in different boreal lake types, *Biogeosciences*, 6(2), 209–223,
993 doi:10.5194/bg-6-209-2009, 2009.
- 994 Kankaala, P., Huotari, J., Tulonen, T. and Ojala, A.: Lake-size dependent physical forcing drives carbon
995 dioxide and methane effluxes from lakes in a boreal landscape, *Limnol. Oceanogr.*, 58(6), 1915–1930,
996 doi:10.4319/lo.2013.58.6.1915, 2013.
- 997 Karlsson, J., Christensen, T. R., Crill, P., Förster, J., Hammarlund, D., Jackowicz-Korczynski, M., Kokfelt, U.,
998 Roehm, C. and Rosén, P.: Quantifying the relative importance of lake emissions in the carbon budget of a
999 subarctic catchment, *J. Geophys. Res.*, 115(G3), G03006, doi:10.1029/2010JG001305, 2010.
- 1000 Katul, G., Mammarella, I., Grönholm, T. and Vesala, T.: A Structure Function Model Recovers the Many
1001 Formulations for Air-Water Gas Transfer Velocity, *Water Resour. Res.*, 54(9), 5905–5920,
1002 doi:10.1029/2018WR022731, 2018.
- 1003 Kell, G. S.: Density, thermal expansivity, and compressibility of liquid water from 0.deg. to 150.deg..
1004 Correlations and tables for atmospheric pressure and saturation reviewed and expressed on 1968
1005 temperature scale, *J. Chem. Eng. Data*, 20(1), 97–105, doi:10.1021/je60064a005, 1975.
- 1006 Koebsch, F., Jurasinski, G., Koch, M., Hofmann, J. and Glatzel, S.: Controls for multi-scale temporal
1007 variation in ecosystem methane exchange during the growing season of a permanently inundated fen,
1008 *Agric. For. Meteorol.*, 204, 94–105, doi:10.1016/j.agrformet.2015.02.002, 2015.
- 1009 Kokfelt, U., Reuss, N., Struyf, E., Sonesson, M., Rundgren, M., Skog, G., Rosén, P. and Hammarlund, D.:
1010 Wetland development, permafrost history and nutrient cycling inferred from late Holocene peat and lake
1011 sediment records in subarctic Sweden, *J. Paleolimnol.*, 44(1), 327–342, doi:10.1007/s10933-010-9406-8,
1012 2010.
- 1013 Lamont, J. C. and Scott, D. S.: An eddy cell model of mass transfer into the surface of a turbulent liquid,
1014 *AIChE J.*, 16(4), 513–519, doi:10.1002/aic.690160403, 1970.
- 1015 Laurion, I., Vincent, W. F., MacIntyre, S., Retamal, L., Dupont, C., Francus, P. and Pienitz, R.: Variability in
1016 greenhouse gas emissions from permafrost thaw ponds, *Limnol. Oceanogr.*, 55(1), 115–133,
1017 doi:10.4319/lo.2010.55.1.0115, 2010.
- 1018 Lofton, D. D., Whalen, S. C. and Hershey, A. E.: Effect of temperature on methane dynamics and
1019 evaluation of methane oxidation kinetics in shallow Arctic Alaskan lakes, *Hydrobiologia*, 721(1), 209–222,
1020 doi:10.1007/s10750-013-1663-x, 2014.
- 1021 Loken, L. C., Crawford, J. T., Schramm, P. J., Stadler, P., Desai, A. R. and Stanley, E. H.: Large spatial and
1022 temporal variability of carbon dioxide and methane in a eutrophic lake, *J. Geophys. Res. Biogeosciences*,
1023 2019JG005186, doi:10.1029/2019JG005186, 2019.
- 1024 López Bellido, J., Tulonen, T., Kankaala, P. and Ojala, A.: CO₂ and CH₄ fluxes during spring and autumn
1025 mixing periods in a boreal lake (Pääjärvi, southern Finland), *J. Geophys. Res.*, 114(G4), G04007,
1026 doi:10.1029/2009JG000923, 2009.
- 1027 Lundin, E. J., Giesler, R., Persson, A., Thompson, M. S. and Karlsson, J.: Integrating carbon emissions from
1028 lakes and streams in a subarctic catchment, *J. Geophys. Res. Biogeosciences*, 118(3), 1200–1207,
1029 doi:10.1002/jgrg.20092, 2013.
- 1030 Lundin, E. J., Klaminder, J., Giesler, R., Persson, A., Olefeldt, D., Heliasz, M., Christensen, T. R. and
1031 Karlsson, J.: Is the subarctic landscape still a carbon sink? Evidence from a detailed catchment balance,



- 1032 Geophys. Res. Lett., 43(5), 1988–1995, doi:10.1002/2015GL066970, 2016.
- 1033 MacIntyre, S. and Melack, J. M.: Vertical and Horizontal Transport in Lakes: Linking Littoral, Benthic, and
1034 Pelagic Habitats, *J. North Am. Benthol. Soc.*, 14(4), 599–615, doi:10.2307/1467544, 1995.
- 1035 MacIntyre, S. and Melack, J. M.: Mixing Dynamics in Lakes Across Climatic Zones, in *Encyclopedia of*
1036 *Inland Waters*, pp. 603–612, Elsevier., 2009.
- 1037 MacIntyre, S., Wanninkhof, R. and Chanton, J. P.: Trace gas exchange across the air–water interface in
1038 freshwater and coastal marine environments, in *Biogenic trace gases: Measuring emissions from soil and*
1039 *water*, pp. 52–97., 1995.
- 1040 MacIntyre, S., Romero, J. R. and Kling, G. W.: Spatial-temporal variability in surface layer deepening and
1041 lateral advection in an embayment of Lake Victoria, East Africa, *Limnol. Oceanogr.*, 47(3), 656–671,
1042 doi:10.4319/lo.2002.47.3.0656, 2002.
- 1043 MacIntyre, S., Fram, J. P., Kushner, P. J., Bettez, N. D., O’Brien, W. J., Hobbie, J. E. and Kling, G. W.:
1044 Climate-related variations in mixing dynamics in an Alaskan arctic lake, *Limnol. Oceanogr.*, 54(6part2),
1045 2401–2417, doi:10.4319/lo.2009.54.6_part_2.2401, 2009.
- 1046 MacIntyre, S., Jonsson, A., Jansson, M., Aberg, J., Turney, D. E. and Miller, S. D.: Buoyancy flux,
1047 turbulence, and the gas transfer coefficient in a stratified lake, *Geophys. Res. Lett.*, 37(24),
1048 doi:10.1029/2010GL044164, 2010.
- 1049 MacIntyre, S., Romero, J. R., Silsbe, G. M. and Emery, B. M.: Stratification and horizontal exchange in
1050 Lake Victoria, East Africa, *Limnol. Oceanogr.*, 59(6), 1805–1838, doi:10.4319/lo.2014.59.6.1805, 2014.
- 1051 MacIntyre, S., Crowe, A. T., Cortés, A. and Arneborg, L.: Turbulence in a small arctic pond, *Limnol.*
1052 *Oceanogr.*, 63(6), 2337–2358, doi:10.1002/lno.10941, 2018.
- 1053 Malmer, N., Johansson, T., Olsrud, M. and Christensen, T. R.: Vegetation, climatic changes and net
1054 carbon sequestration in a North-Scandinavian subarctic mire over 30 years, *Glob. Chang. Biol.*, 11, 1895–
1055 1909, doi:10.1111/j.1365-2486.2005.01042.x, 2005.
- 1056 Mammarella, I., Nordbo, A., Rannik, Ü., Haapanala, S., Levula, J., Laakso, H., Ojala, A., Peltola, O.,
1057 Heiskanen, J., Pumpanen, J. and Vesala, T.: Carbon dioxide and energy fluxes over a small boreal lake in
1058 Southern Finland, *J. Geophys. Res. Biogeosciences*, 120(7), 1296–1314, doi:10.1002/2014JG002873,
1059 2015.
- 1060 Markfort, C. D., Perez, A. L. S., Thill, J. W., Jaster, D. A., Porté-Agel, F. and Stefan, H. G.: Wind sheltering of
1061 a lake by a tree canopy or bluff topography, *Water Resour. Res.*, 46(3), 1–13,
1062 doi:10.1029/2009WR007759, 2010.
- 1063 Matthews, C. J. D., St.Louis, V. L. and Hesslein, R. H.: Comparison of Three Techniques Used To Measure
1064 Diffusive Gas Exchange from Sheltered Aquatic Surfaces, *Environ. Sci. Technol.*, 37(4), 772–780,
1065 doi:10.1021/es0205838, 2003.
- 1066 McCalley, C. K., Woodcroft, B. J., Hodgkins, S. B., Wehr, R. A., Kim, E.-H., Mondav, R., Crill, P. M., Chanton,
1067 J. P., Rich, V. I., Tyson, G. W. and Saleska, S. R.: Methane dynamics regulated by microbial community
1068 response to permafrost thaw, *Nature*, 514(7523), 478–481, doi:10.1038/nature13798, 2014.
- 1069 McGinnis, D. F., Kirillin, G., Tang, K. W., Flury, S., Bodmer, P., Engelhardt, C., Casper, P. and Grossart, H.-
1070 P.: Enhancing surface methane fluxes from an oligotrophic lake: exploring the microbubble hypothesis.,
1071 *Environ. Sci. Technol.*, 49(2), 873–80, doi:10.1021/es503385d, 2015.



- 1072 Merlivat, L. and Memery, L.: Gas exchange across an air-water interface: Experimental results and
1073 modeling of bubble contribution to transfer, *J. Geophys. Res.*, 88(C1), 707,
1074 doi:10.1029/JC088iC01p00707, 1983.
- 1075 Miettinen, H., Pumpanen, J., Heiskanen, J. J., Aaltonen, H., Mammarella, I., Ojala, A., Levula, J. and
1076 Rantakari, M.: Towards a more comprehensive understanding of lacustrine greenhouse gas dynamics —
1077 two-year measurements of concentrations and fluxes of CO₂, CH₄ and N₂O in a typical boreal ..., *Boreal*
1078 *Environ. Res.*, 6095(December), 75–89, 2015.
- 1079 Murase, J., Sakai, Y., Sugimoto, A., Okubo, K. and Sakamoto, M.: Sources of dissolved methane in Lake
1080 Biwa, *Limnology*, 4(2), 91–99, doi:10.1007/s10201-003-0095-0, 2003.
- 1081 Natchimuthu, S., Sundgren, I., Gålfalk, M., Klemedtsson, L., Crill, P., Danielsson, Å. and Bastviken, D.:
1082 Spatio-temporal variability of lake CH₄ fluxes and its influence on annual whole lake emission estimates,
1083 *Limnol. Oceanogr.*, 61(S1), S13–S26, doi:10.1002/lno.10222, 2016.
- 1084 Natchimuthu, S., Sundgren, I., Gålfalk, M., Klemedtsson, L. and Bastviken, D.: Spatiotemporal variability
1085 of lake pCO₂ and CO₂ fluxes in a hemiboreal catchment, *J. Geophys. Res. Biogeosciences*, 122(1), 30–
1086 49, doi:10.1002/2016JG003449, 2017.
- 1087 Ojala, A., Bellido, J. L., Tulonen, T., Kankaala, P. and Huotari, J.: Carbon gas fluxes from a brown-water
1088 and a clear-water lake in the boreal zone during a summer with extreme rain events, *Limnol. Oceanogr.*,
1089 56(1), 61–76, doi:10.4319/lo.2011.56.1.0061, 2011.
- 1090 Olefeldt, D. and Roulet, N. T.: Effects of permafrost and hydrology on the composition and transport of
1091 dissolved organic carbon in a subarctic peatland complex, *J. Geophys. Res. Biogeosciences*, 117(G1), 1–
1092 15, doi:10.1029/2011JG001819, 2012.
- 1093 Olefeldt, D., Roulet, N. T., Bergeron, O., Crill, P., Bäckstrand, K. and Christensen, T. R.: Net carbon
1094 accumulation of a high-latitude permafrost palsa mire similar to permafrost-free peatlands, *Geophys.*
1095 *Res. Lett.*, 39(3), n/a-n/a, doi:10.1029/2011GL050355, 2012.
- 1096 Pappas, C., Mahecha, M. D., Frank, D. C., Babst, F. and Koutsoyiannis, D.: Ecosystem functioning is
1097 enveloped by hydrometeorological variability, *Nat. Ecol. Evol.*, 1(9), 1263–1270, doi:10.1038/s41559-
1098 017-0277-5, 2017.
- 1099 Paytan, A., Lecher, A. L., Dimova, N., Sparrow, K. J., Kodovska, F. G.-T., Murray, J., Tulaczyk, S. and
1100 Kessler, J. D.: Methane transport from the active layer to lakes in the Arctic using Toolik Lake, Alaska, as a
1101 case study, *Proc. Natl. Acad. Sci.*, 112(12), 201417392, doi:10.1073/pnas.1417392112, 2015.
- 1102 Podgrajsek, E., Sahlée, E., Bastviken, D., Holst, J., Lindroth, A., Tranvik, L. and Rutgersson, A.: Comparison
1103 of floating chamber and eddy covariance measurements of lake greenhouse gas fluxes, *Biogeosciences*,
1104 11(15), 4225–4233, doi:10.5194/bg-11-4225-2014, 2014a.
- 1105 Podgrajsek, E., Sahlée, E. and Rutgersson, A.: Diurnal cycle of lake methane flux, *J. Geophys. Res.*
1106 *Biogeosciences*, 119(3), 236–248, doi:10.1002/2013JG002327, 2014b.
- 1107 Podgrajsek, E., Sahlée, E. and Rutgersson, A.: Diel cycle of lake-air CO₂ flux from a shallow lake and the
1108 impact of waterside convection on the transfer velocity, *J. Geophys. Res. Biogeosciences*, 120(1), 29–38,
1109 doi:10.1002/2014JG002781, 2015.
- 1110 Poindexter, C. M., Baldocchi, D. D., Matthes, J. H., Knox, S. H. and Variano, E. A.: The contribution of an
1111 overlooked transport process to a wetland's methane emissions, *Geophys. Res. Lett.*, 43(12), 6276–6284,



- 1112 doi:10.1002/2016GL068782, 2016.
- 1113 Prairie, Y. and del Giorgio, P.: A new pathway of freshwater methane emissions and the putative
1114 importance of microbubbles, *Int. Waters*, 3(3), 311–320, doi:10.5268/IW-3.3.542, 2013.
- 1115 Rantala, M. V., Nevalainen, L., Rautio, M., Galkin, A. and Luoto, T. P.: Sources and controls of organic
1116 carbon in lakes across the subarctic treeline, *Biogeochemistry*, 129(1–2), 235–253, doi:10.1007/s10533-
1117 016-0229-1, 2016.
- 1118 Rasilo, T., Prairie, Y. T. and del Giorgio, P. A.: Large-scale patterns in summer diffusive CH₄ fluxes across
1119 boreal lakes, and contribution to diffusive C emissions, *Glob. Chang. Biol.*, 21(3), 1124–1139,
1120 doi:10.1111/gcb.12741, 2015.
- 1121 Read, J. S., Hamilton, D. P., Desai, A. R., Rose, K. C., MacIntyre, S., Lenters, J. D., Smyth, R. L., Hanson, P.
1122 C., Cole, J. J., Staehr, P. A., Rusak, J. A., Pierson, D. C., Brookes, J. D., Laas, A. and Wu, C. H.: Lake-size
1123 dependency of wind shear and convection as controls on gas exchange, *Geophys. Res. Lett.*, 39(9),
1124 doi:10.1029/2012GL051886, 2012.
- 1125 Ribas-Ribas, M., Kilcher, L. F. and Wurl, O.: *Sniffle*: a step forward to measure *in situ* CO₂ fluxes with the
1126 floating chamber technique, *Elem Sci Anth*, 6(1), 14, doi:10.1525/elementa.275, 2018.
- 1127 Rueda, F., Moreno-Ostos, E. and Cruz-Pizarro, L.: Spatial and temporal scales of transport during the
1128 cooling phase of the ice-free period in a small high-mountain lake, *Aquat. Sci.*, 69(1), 115–128,
1129 doi:10.1007/s00027-006-0823-8, 2007.
- 1130 Schilder, J., Bastviken, D., van Hardenbroek, M., Kankaala, P., Rinta, P., Stötter, T. and Heiri, O.: Spatial
1131 heterogeneity and lake morphology affect diffusive greenhouse gas emission estimates of lakes,
1132 *Geophys. Res. Lett.*, 40(21), 5752–5756, doi:10.1002/2013GL057669, 2013.
- 1133 Schilder, J., Bastviken, D., van Hardenbroek, M. and Heiri, O.: Spatiotemporal patterns in methane flux
1134 and gas transfer velocity at low wind speeds: Implications for upscaling studies on small lakes, *J.*
1135 *Geophys. Res. Biogeosciences*, 121(6), 1456–1467, doi:10.1002/2016JG003346, 2016.
- 1136 Sepulveda-Jauregui, A., Walter Anthony, K. M., Martinez-Cruz, K., Greene, S. and Thalasso, F.: Methane
1137 and carbon dioxide emissions from 40 lakes along a north–south latitudinal transect in Alaska,
1138 *Biogeosciences*, 12(11), 3197–3223, doi:10.5194/bg-12-3197-2015, 2015.
- 1139 Sheskin, D. J.: *Handbook of Parametric and Nonparametric Statistical Procedures*, 4th ed., Chapman &
1140 Hall/CRC., 2007.
- 1141 Smith, S. D.: Coefficients for sea surface wind stress, heat flux, and wind profiles as a function of wind
1142 speed and temperature, *J. Geophys. Res.*, 93(C12), 15467, doi:10.1029/JC093iC12p15467, 1988.
- 1143 Soumis, N., Canuel, R. and Lucotte, M.: Evaluation of Two Current Approaches for the Measurement of
1144 Carbon Dioxide Diffusive Fluxes from Lentic Ecosystems, *Environ. Sci. Technol.*, 42(8), 2964–2969,
1145 doi:10.1021/es702361s, 2008.
- 1146 Tan, Z. and Zhuang, Q.: Methane emissions from pan-Arctic lakes during the 21st century: An analysis
1147 with process-based models of lake evolution and biogeochemistry, *J. Geophys. Res. Biogeosciences*,
1148 120(12), 2641–2653, doi:10.1002/2015JG003184, 2015.
- 1149 Tedford, E. W., MacIntyre, S., Miller, S. D. and Czikowsky, M. J.: Similarity scaling of turbulence in a
1150 temperate lake during fall cooling, *J. Geophys. Res. Ocean.*, 119(8), 4689–4713,
1151 doi:10.1002/2014JC010135, 2014.



- 1152 Terray, E. A., Donelan, M. A., Agrawal, Y. C., Drennan, W. M., Kahma, K. K., Williams, A. J., Hwang, P. A.
1153 and Kitaigorodskii, S. A.: Estimates of Kinetic Energy Dissipation under Breaking Waves, *J. Phys.*
1154 *Oceanogr.*, 26(5), 792–807, doi:10.1175/1520-0485(1996)026<0792:EOKEDU>2.0.CO;2, 1996.
- 1155 Theofanous, T. G., Houze, R. N. and Brumfield, L. K.: Turbulent mass transfer at free, gas-liquid interfaces,
1156 with applications to open-channel, bubble and jet flows, *Int. J. Heat Mass Transf.*, 19(6), 613–624,
1157 doi:10.1016/0017-9310(76)90044-2, 1976.
- 1158 Thornton, B. F., Wik, M. and Crill, P. M.: Climate-forced changes in available energy and methane
1159 bubbling from subarctic lakes, *Geophys. Res. Lett.*, 42(6), 1936–1942, doi:10.1002/2015GL063189, 2015.
- 1160 Tokoro, T., Kayanne, H., Watanabe, A., Nadaoka, K., Tamura, H., Nozaki, K., Kato, K. and Negishi, A.: High
1161 gas-transfer velocity in coastal regions with high energy-dissipation rates, *J. Geophys. Res.*, 113(C11),
1162 C11006, doi:10.1029/2007JC004528, 2008.
- 1163 Turner, W. R.: Microbubble Persistence in Fresh Water, *J. Acoust. Soc. Am.*, 33(9), 1223–1233,
1164 doi:10.1121/1.1908960, 1961.
- 1165 Tveit, A. T., Urich, T., Frenzel, P. and Svenning, M. M.: Metabolic and trophic interactions modulate
1166 methane production by Arctic peat microbiota in response to warming, *Proc. Natl. Acad. Sci.*, 112(19),
1167 E2507–E2516, doi:10.1073/pnas.1420797112, 2015.
- 1168 Tyrllis, E. and Hoskins, B. J.: Aspects of a Northern Hemisphere Atmospheric Blocking Climatology, *J.*
1169 *Atmos. Sci.*, 65(5), 1638–1652, doi:10.1175/2007JAS2337.1, 2008.
- 1170 Vachon, D. and Prairie, Y. T.: The ecosystem size and shape dependence of gas transfer velocity versus
1171 wind speed relationships in lakes, edited by R. Smith, *Can. J. Fish. Aquat. Sci.*, 70(12), 1757–1764,
1172 doi:10.1139/cjfas-2013-0241, 2013.
- 1173 Vachon, D., Prairie, Y. T. and Cole, J. J.: The relationship between near-surface turbulence and gas
1174 transfer velocity in freshwater systems and its implications for floating chamber measurements of gas
1175 exchange, *Limnol. Oceanogr.*, 55(4), 1723–1732, doi:10.4319/lo.2010.55.4.1723, 2010.
- 1176 Vachon, D., Langenegger, T., Donis, D. and McGinnis, D. F.: Influence of water column stratification and
1177 mixing patterns on the fate of methane produced in deep sediments of a small eutrophic lake, *Limnol.*
1178 *Oceanogr.*, Ino.11172, doi:10.1002/Ino.11172, 2019.
- 1179 Wang, B., Liao, Q., Fillingham, J. H. and Bootsma, H. A.: On the coefficients of small eddy and surface
1180 divergence models for the air-water gas transfer velocity, *J. Geophys. Res. Ocean.*, 120(3), 2129–2146,
1181 doi:10.1002/2014JC010253, 2015.
- 1182 Wanninkhof, R.: Relationship between wind speed and gas exchange over the ocean, *J. Geophys. Res.*,
1183 97(C5), 7373, doi:10.1029/92JC00188, 1992.
- 1184 Wanninkhof, R.: Relationship between wind speed and gas exchange over the ocean revisited, *Limnol.*
1185 *Oceanogr. Methods*, 12(6), 351–362, doi:10.4319/lom.2014.12.351, 2014.
- 1186 Weyhenmeyer, G. A., Kosten, S., Wallin, M. B., Tranvik, L. J., Jeppesen, E. and Roland, F.: Significant
1187 fraction of CO₂ emissions from boreal lakes derived from hydrologic inorganic carbon inputs, *Nat.*
1188 *Geosci.*, 8(12), 933–936, doi:10.1038/ngeo2582, 2015.
- 1189 Wiesenburg, D. A. and Guinasso, N. L.: Equilibrium solubilities of methane, carbon monoxide, and
1190 hydrogen in water and sea water, *J. Chem. Eng. Data*, 24(4), 356–360, doi:10.1021/je60083a006, 1979.



- 1191 Wik, M., Crill, P. M., Bastviken, D., Danielsson, Å. and Norbäck, E.: Bubbles trapped in arctic lake ice:
1192 Potential implications for methane emissions, *J. Geophys. Res.*, 116(G3), G03044,
1193 doi:10.1029/2011JG001761, 2011.
- 1194 Wik, M., Crill, P. M., Varner, R. K. and Bastviken, D.: Multiyear measurements of ebullitive methane flux
1195 from three subarctic lakes, *J. Geophys. Res. Biogeosciences*, 118(3), 1307–1321, doi:10.1002/jgrg.20103,
1196 2013.
- 1197 Wik, M., Thornton, B. F., Bastviken, D., MacIntyre, S., Varner, R. K. and Crill, P. M.: Energy input is primary
1198 controller of methane bubbling in subarctic lakes, *Geophys. Res. Lett.*, 41(2), 555–560,
1199 doi:10.1002/2013GL058510, 2014.
- 1200 Wik, M., Thornton, B. F., Bastviken, D., Uhlbäck, J. and Crill, P. M.: Biased sampling of methane release
1201 from northern lakes: A problem for extrapolation, *Geophys. Res. Lett.*, 43(3), 1256–1262,
1202 doi:10.1002/2015GL066501, 2016a.
- 1203 Wik, M., Varner, R. K., Walter Anthony, K. M., MacIntyre, S. and Bastviken, D.: Climate-sensitive northern
1204 lakes and ponds are critical components of methane release, *Nat. Geosci.*, 9(2), 99–105,
1205 doi:10.1038/ngeo2578, 2016b.
- 1206 Wik, M., Johnson, J. E., Crill, P. M., DeStasio, J. P., Erickson, L., Halloran, M. J., Fahnestock, M. F.,
1207 Crawford, M. K., Phillips, S. C. and Varner, R. K.: Sediment Characteristics and Methane Ebullition in
1208 Three Subarctic Lakes, *J. Geophys. Res. Biogeosciences*, 123(8), 2399–2411, doi:10.1029/2017JG004298,
1209 2018.
- 1210 Woolf, D. K. and Thorpe, S. A.: Bubbles and the air-sea exchange of gases in near-saturation conditions, *J.*
1211 *Mar. Res.*, 49(3), 435–466, doi:10.1357/002224091784995765, 1991.
- 1212 Yvon-Durocher, G., Allen, A. P., Bastviken, D., Conrad, R., Gudas, C., St-Pierre, A., Thanh-Duc, N. and del
1213 Giorgio, P. A.: Methane fluxes show consistent temperature dependence across microbial to ecosystem
1214 scales, *Nature*, 507(7493), 488–491, doi:10.1038/nature13164, 2014.
- 1215 Yvon-Durocher, G., Hulatt, C. J., Woodward, G. and Trimmer, M.: Long-term warming amplifies shifts in
1216 the carbon cycle of experimental ponds, *Nat. Clim. Chang.*, 7(3), 209–213, doi:10.1038/nclimate3229,
1217 2017.
- 1218 Zappa, C. J., McGillis, W. R., Raymond, P. A., Edson, J. B., Hints, E. J., Zemmelen, H. J., Dacey, J. W. H.
1219 and Ho, D. T.: Environmental turbulent mixing controls on air-water gas exchange in marine and aquatic
1220 systems, *Geophys. Res. Lett.*, 34(10), L10601, doi:10.1029/2006GL028790, 2007.
- 1221 Zimov, S. A., Voropaev, Y. V., Semiletov, I. P., Davidov, S. P., Prosiannikov, S. F., Chapin, M. C., Chapin III,
1222 F. S., Trumbore, S. and Tyler, S.: North Siberian Lakes: A Methane Source Fueled by Pleistocene Carbon,
1223 *Science* (80-.), 277(5327), 800–802, doi:10.1126/science.277.5327.800, 1997.
- 1224